

Algorithm Technical Background Document

VIIRS Land Surface Phenology Product

(Version 1.0, 31 October 2016)

Investigators: Xiaoyang Zhang, Mark A. Friedl, and Geoffrey M. Henebry

Collaborators: Crystal Schaaf, and Tomoaki Miura

(VIIRS Science Team)

ABSTRACT

Growing evidence has emerged that climate change-induced shifts in phenology are having substantial impacts on ecosystem function, biodiversity, and carbon budgets at multiple scales. Timing of leaf-on and leaf-off periods also affects land surface albedo, exerting a strong control on surface radiation budgets and the partitioning of net radiation between latent and sensible heat fluxes. As a result, there is a critical need to produce accurate and timely global land surface phenology data sets.

The goal of the VIIRS global land surface phenology (GLSP) product is to develop science quality standard data products that will enable continuity of a key standard Earth system data record from VIIRS data. This product will provide consistent spatial and temporal estimates of the timing and magnitude of vegetation phenological development across the globe, and will be suitable for characterizing and understanding interannual-to-decadal scale changes in ecosystem response to climate change.

The VIIRS GLSP algorithm uses daily VIIRS Nadir BRDF (bidirectional reflectance distribution function)-Adjusted reflectances (NBAR) in combination with VIIRS land surface temperature, snow cover, and land cover type at each pixel as inputs. The VIIRS NBAR product is used to generate time series of the two band enhanced vegetation index at each 500m gridded pixel. The VIIRS GLSP will be produced once a year, and will provide twelve phenological metrics (seven phenological dates and five phenological magnitudes), along with quality assurance flags and metrics characterizing the confidence of phenology retrievals at each pixel.

Table of Contents

1.	Introduction.....	4
2.	Background.....	4
2.1.	State of the Science	4
2.2.	Existing Algorithms and Products.....	6
3.	VIIRS Global Land Surface Phenology.....	7
3.1.	Product Overview.....	7
3.2.	VIIRS Land Surface Phenology Algorithm	8
4.	Input Data and Preprocessing.....	12
4.1.	Input data.....	12
4.2.	Smoothing and Gap Filling	13
4.3.	Snow-Contamination and Assignment of Background EVI2 Values.....	14
5.	Related Technical Issues and Considerations	14
5.1.	Back-Up EVI2 Values	14
5.2.	Limitations to Land Surface Phenology Retrievals	15
5.3.	Geographic Variability in Growing Season Timing	15
6.	VIIRS GLSP Quality Assurance	16
7.	Product Implementation and Initial Accuracy Assessment.....	18
7.1.	VIIRS GLSP algorithm Results in North America.....	19
7.2.	Evaluation of VIIRS GLSP	20
8.	Land Surface Phenology Specification.....	25
8.1.	Science Data Records	26
8.2.	Product Specification.....	31
9.	Literature Cited	32

1. Introduction

Vegetation phenology is a sensitive indicator of biological responses to climate change (Cleland et al. 2012; Ivits et al. 2012; Morisette et al. 2009). Long-term records of vegetation phenology observed from both species-specific *in-situ* and from satellite observations have greatly contributed to improve understanding of the biological responses to climate change at regional to global scales (Cleland et al. 2007; Korner and Basler 2010; Parmesan and Yohe 2003; Richardson et al. 2013; Walther 2010). Vegetation phenology is readily observable and easily understood by the public; thus, it is widely acknowledged to be a key indicator that can be used to track ecosystem changes in response to climate change by the Intergovernmental Panel on Climate Change (IPCC 2007, 2014), the United States Global Change Research Program (USGCRP 2010, 2015), and the Environmental Protection Agency (EPA 2016).

The phenological dynamics of vegetated ecosystems also influence a host of ecophysiological processes that affect hydrologic processes (Gerten et al. 2004; Hogg et al. 2000; Vivoni 2012), biogeochemistry and nutrient cycling (Campbell et al. 2009; Cooke and Weih 2005), and land-atmosphere interactions (Heimann et al. 1998; Puma et al. 2013). Indeed, vegetation phenology affects terrestrial carbon cycling across a wide range of ecosystem and climatic regimes (Baldocchi et al. 2001; Churkina et al. 2005; Gray et al. 2014; Richardson et al. 2009b). The presence and absence of leaves affects land surface albedo (Moore et al. 1996; Ollinger et al. 2008; Williamson et al. 2016) and exerts strong control on surface radiation budgets and the partitioning of net radiation between latent and sensible heat fluxes (Chen and Dudhia 2001; Vivoni 2012). Therefore, investigations focused on monitoring climate change and modeling biospheric processes require accurate and timely information related to spatiotemporal dynamics of vegetation phenology. While some data sets related to the phenology of particular plant species have been collected at specific sites and across networks, remote sensing provides the only way to observe and monitor phenological dynamics at landscape to global scales and at regular intervals.

The VIIRS (Visible Infrared Imaging Radiometer Suite) Global Land Surface Phenology (GLSP) Product is being developed to meet the science and applications community needs for consistent and global records of land surface phenology. The product is based on established algorithms for estimating a long term record of global land surface phenology, and is being designed to provide continuity with the MODIS (Moderate-resolution Imaging Spectroradiometer) Global Land Cover Dynamics Product (MCD12Q2; Zhang et al., 2006; Ganguly et al., 2010). Before describing the VIIRS GLSP algorithm and product specification, we will first provide a brief overview of the current state of the science.

2. Background

2.1. State of the Science

In recent decades, growing season dynamics, including shifts in the timing of bud burst, leaf development, senescence, and changes in growing season length, have been widely studied in the context of ecosystem responses to climate change (Parmesan and Yohe 2003). Complex phenological responses have also been observed in controlled experiments where

warming was shown to accelerate the phenology of plant canopies (Cleland et al. 2012; Wolkovich et al. 2012), but elevated CO₂ and nitrogen fertilization delayed flowering (Cleland et al. 2007). These biophysical and biochemical processes both influence and are diagnostic of ecosystem-climate interactions. As a consequence, there is a substantial need to accurately characterize the phenology of ecosystems, and by extension, the response of ecosystems to changes in the climate (Morissette et al. 2009). Many data sets related to plant phenology have been (or are being) collected at specific field sites or in networks focused on individual plants or plant species. However, because of the geographical and temporal sampling of these data sets, synthesis of such observations, to characterize regional to global scale patterns and dynamics in phenology, is extremely difficult.

Moderate resolution satellite remote sensing provides global high temporal frequency measurements of land surface properties, and are therefore well-suited for monitoring seasonal-to-decadal patterns and trends in regional-to-global phenology (de Beurs and Henebry 2005a; Henebry and de Beurs 2013; Reed et al. 1994b; White et al. 1997; Zhang et al. 2003; Zhang et al. 2014). Phenological timing and magnitude derived from satellite data are estimated from temporal dynamics in vegetation indices and therefore do not provide directly observed features of plant phenology. Hence, remotely sensed observations of phenological dynamics are often referred to as “land surface phenology” (de Beurs and Henebry 2004; Henebry and de Beurs 2013). Indeed, the utility of coarse and moderate spatial resolution sensors for studies of land surface phenology has been well established over the last 20 years (de Beurs and Henebry 2005b; de Beurs and Henebry 2010; Justice et al. 1985; Reed et al. 1994a; White et al. 1997; Zhang et al. 2003). Landsat MSS was the first space-borne sensor used to characterize the seasonality of vegetation at landscape and regional scales (Thompson and Wehmanen 1979). However, detecting phenological transition dates requires higher temporal resolution than is currently afforded by Landsat-class instruments, so moderate spatial resolution sensors such as the Advanced Very High Resolution Radiometer (AVHRR) (Goward et al. 1985), MODIS (Zhang et al., 2003), and SPOT-VEGETATION (Delbart et al. 2005) are more commonly used for this purpose.

The utility of remote sensing time series for phenology-related studies has been widely demonstrated during last two decades. Specifically, by exploiting the growing archive of global optical satellite data, especially from AVHRR, MODIS and SPOT, a number of studies have revealed important spatial and temporal patterns in the time series of moderate to coarse resolution vegetation indices. Prominent examples include studies using AVHRR showing that northern hemisphere temperate and boreal regions (~40°-70° N) experienced increased growing season greenness related to surface warming during the period 1981 to 1999 (Myneni et al. 1997; Zhou et al. 2001). More recent studies, utilizing a longer record of AVHRR data, suggest a more complex pattern with evidence of “browning” trends in the boreal forests of Southern Alaska, Canada, and in the interior of Russia (Angert et al. 2005; de Jong et al. 2011; Goetz et al. 2005; Zhang et al. 2007) and complicated impacts of climate modes on land surface phenology in the Northern Hemisphere (de Beurs and Henebry 2008; Zhang et al. 2007). Similar studies, conducted for tropical regions, suggest significant “greening” in regions such as the Sahel, associated with long-term trends in precipitation regimes (Herrmann et al. 2005; Hickler et al. 2005; Olsson et al. 2005; Seaquist et al. 2006). Despite their wide use, AVHRR data are not well suited for most vegetation monitoring applications because the sensors lack precise radiometric calibration, exhibit poor geometric

registration, and use spatial resampling methods that decrease their utility (Goward et al. 1991).

The availability of the MODIS data since 2000 provides a substantially improved global remote sensing data source with dramatically improved radiometric and geometric properties, atmospheric correction, and cloud screening, thereby enabling more reliable and consistent characterization of land surface phenology at spatial resolutions from 250 m to 1000 m (Ganguly et al. 2010; Tan et al. 2011; Zhang et al. 2006). Recently, MODIS phenology has been used to identify enhancement of ecosystem carbon uptake (Keenan et al. 2014b), and to characterize climate change impacts in tropical forests (Huete et al. 2006; Zhou et al. 2014), arctic ecosystems (Zeng et al. 2013), and at global scales (Zhang et al. 2014). However, the MODIS sensors are aging and near the end of their current duty cycles. The VIIRS sensors, onboard the Suomi National Polar-orbiting Partnership (NPP) satellite, launched on October 28, 2011, is and will continue to provide a continuity of the MODIS data record (Justice et al. 2013). This ATBD describes the algorithmic basis and product specification for extending the MODIS MCD12Q2 data record into the VIIRS era.

2.2. Existing Algorithms and Products

A number of different approaches have been developed over the last two decades to model the temporal trajectory of vegetation indices and estimate the timing of phenological processes from satellite remote sensing. To reduce the noise in vegetation index (VI) data, the maximum value composite (MVC) (Holben 1986), the constraint view-angle MVC (CVMVC)(van Leeuwen et al. 1999), and best index slope extraction (BISE) (Viovy et al. 1992) methods are commonly applied to create weekly, biweekly, or monthly composites that minimize cloud and atmospheric contamination. To further reduce noise, time series of VI data are often smoothed using a variety of different methods including Fourier harmonic analysis (Moody and Johnson, 2001), asymmetric Gaussian function-fitting (Jonsson and Eklundh, 2002), piece-wise logistic functions (Zhang et al., 2003), Savitzky–Golay filters (Chen et al. 2004), degree-day based convex quadratic models (de Beurs and Henebry 2004; Henebry and de Beurs 2013) and polynomial curve fitting (Bradley et al. 2007).

To produce phenology metrics at regional and global scales from the resulting time series of VI data, a wide array of methods has been developed. The commonly used methods include threshold-based techniques (Jonsson and Eklundh 2002; White et al. 1997), spectral analysis (Jakubauskas et al. 2001; Moody and Johnson 2001), and inflection point estimation in the time series of vegetation indices (Moulin et al. 1997; Zhang et al. 2003). All methods use time series of VI data to identify the timing of phenological metrics such as the start and end of the growing season. However, considerable differences exist in the various phenological detection methods (de Beurs and Henebry 2010; White et al. 2009).

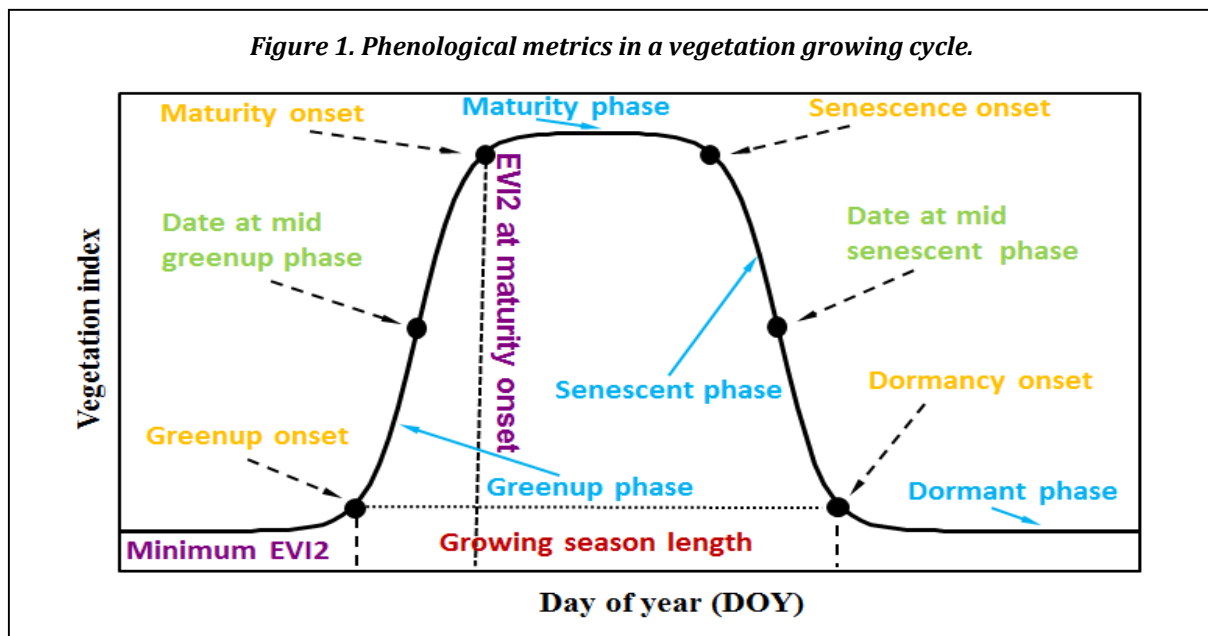
In parallel with these algorithm development activities, a large number of phenology products have been (or are being) developed for use by the community. To date, the MODIS Land Cover Dynamics Product (MCD12Q2) is the only global product that is produced on an operational basis (Ganguly et al. 2010; Zhang et al. 2006). Other products include the MODIS-based product generated at NASA-GSFC in support of the North American Carbon Program (Tan et al. 2011), a product being generated for the Contiguous United States (CONUS) by the US Forest Service (Hargrove et al. 2009), the USGS long-term 1-km AVHRR phenology

product for the CONUS (1989-present; Reed, 1994), the 1 km Europe phenology based on the time-series of Terrestrial Chlorophyll Index (MTCI) from Multi-temporal Medium Resolution Imaging Spectrometer (MERIS) from 2002 to 2012 (Rodriguez-Galiano et al. 2015), a global product based on FPAR developed by the ESA (Verstraete et al. 2008), and a global long-term climate modeling grid (CMG) LSP (LTCMG-LSP) product at a spatial resolution of 0.05°degrees from time series of AVHRR (1982-1999) and MODIS (2000-2015) (Zhang 2015; Zhang et al. 2014). In addition, a large number of land surface phenology products have been generated focused on specific sensors, time periods, and regions for specific application purposes (Bolton and Friedl 2013; Boyd et al. 2011; Krehbiel et al. 2016; Melaas et al. 2013; Melaas et al. 2016).

3. VIIRS Global Land Surface Phenology

3.1. Product Overview

The objective of the VIIRS GLSP product is to produce global datasets that provide quantitative characterization of dynamics in vegetation phenology at a spatial resolution of 500m that provides continuity with the MODIS MCD12Q2 product. To do this, the GLSP product characterizes vegetation growth cycles using four key transition dates estimated from time series of two band enhanced vegetation index (EVI2) data: (1) greenup onset: the date of onset of EVI2 increase; (2) maturity onset: the date of onset of EVI2 maximum; (3) senescence onset: the date of onset of EVI2 decrease; and (4) dormancy onset: the date of onset of EVI2 minimum (Figure 1). These four phenological transition dates divide the vegetation growing cycle into four vegetation growing phases: greenup phase, maturity phase, senescent phase, and dormant phase. In addition, the algorithm also computes dates corresponding to the mid-point of the greenup and senescent phases, EVI2 values at greenup onset and maturity onset, the growing season integrated EVI2 (the sum of the modeled daily EVI2 values from the onset of EVI2 increase to the onset of EVI2 minimum), and the rates of change in EVI2 values during the growth and senescence phases (Table 1) (see Section 8 for



details regarding the product specification). Table 1 summarizes the specification for the data sets and format of the product.

Table 1. VIIRS global land surface phenology metrics. *PGQ is the proportion of good quality EVI2 values.

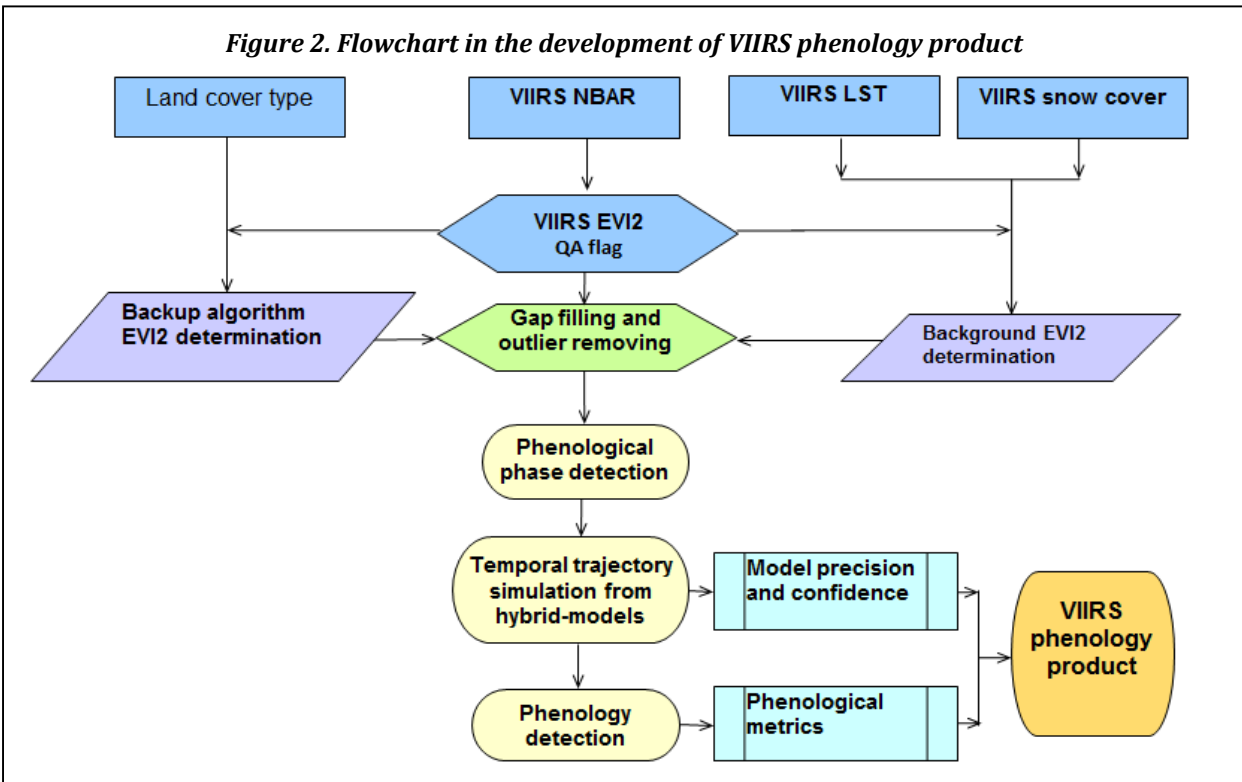
VIIRS phenology Product Fields		Units	Data format
Phenological metrics	<i>Onset of greenness increase</i>	Day of Year (DOY)	Format : uint16 Range : 1 to 32767
	<i>Onset of greenness maximum</i>		
	<i>Onset of greenness decrease</i>		
	<i>Onset of greenness minimum</i>		
	<i>Date at mid greenup phase</i>		
	<i>Date at mid senescent phase</i>		
	<i>Growing season length</i>	Number of Days	Format: uint16 Range: 1 to 365
	<i>EVI2 at onset of greenness increase</i>	EVI2	Format: uint16 Range: 0 to 10,000 Scale: 10,000
	<i>EVI2 at onset of greenness maximum</i>		
	<i>Summation of growing season EVI2 at a giving time</i>	Σ EVI2	Format: uint16 Range: 0 to 32767
<i>Rate of change in greenness increase</i>	Δ EVI2/dT	Format: uint16 Range : 0 to 32767	
<i>Rate of change in greenness decrease</i>			
Confidence*	<i>Greenness agreement in a growing season</i>	N/A	Format: uint8 Range : 0 to 100
	<i>PGQ during a growing season</i>		
	<i>PGQ around onset greenness increase</i>		
	<i>PGQ around onset greenness maximum</i>		
	<i>PGQ around onset greenness decrease</i>		
	<i>PGQ around onset greenness dormancy</i>		
	<i>Phenology quality assurance</i>	N/A	Format: uint8 Bit fields to hold different quality states

3.2. VIIRS Land Surface Phenology Algorithm

The basis for the VIIRS GLSP algorithm is the MODIS land cover dynamics (MLCD) algorithm in collection 5 (Ganguly 2010). The MLCD V005 algorithm currently uses 8-day MODIS Nadir BRDF (bidirectional reflectance distribution function)-Adjusted reflectances (NBAR-MCD43A4) (Schaaf et al. 2002; Schaaf et al. 2011) and MODIS land surface

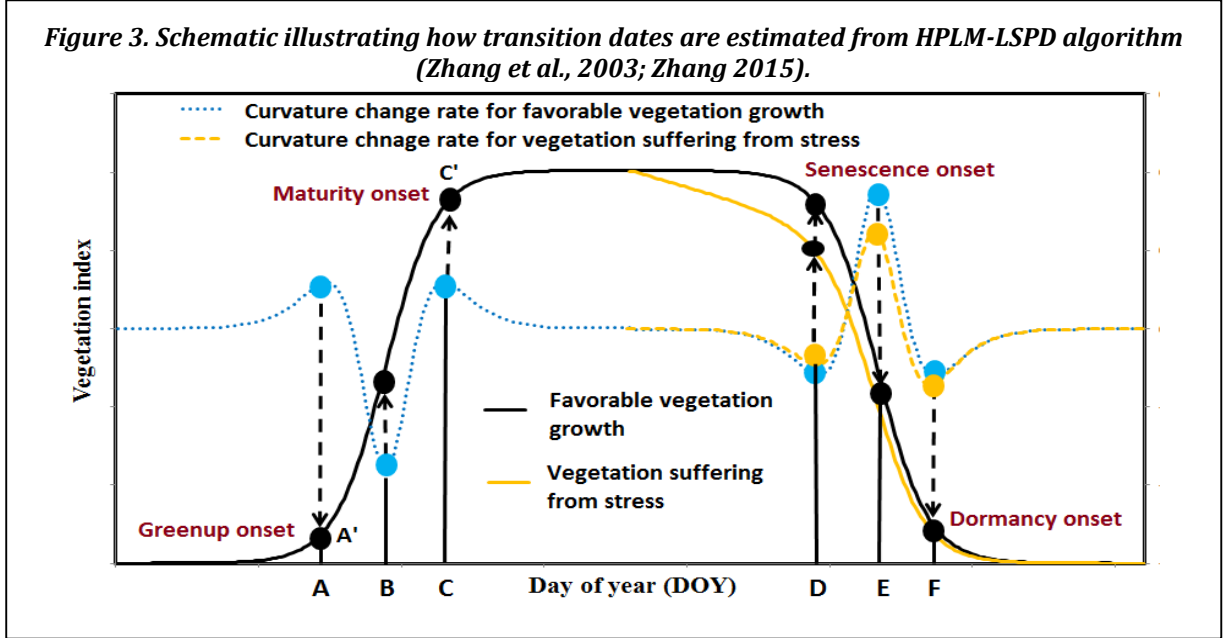
temperature data at each pixel as inputs. In order to generate the VIIRS GLSP product, the MLCD algorithm has been refined to allow for more flexible EVI2 trajectories (Zhang 2015) using daily V006 NBAR values (Wang et al. 2012). Here we provide a description of the algorithm used for the VIIRS GLSP product, including specific refinements that are being developed for the VIIRS product and that are not included in the MCD12Q2 algorithm.

The conceptual basis and processing flow for the VIIRS GLSP product are presented in Figures 2 & 3. Following this framework, estimation of land surface phenology metrics included in the product involves nine main steps, which are listed below (Figure 2):



1. Visible and near infrared VIIRS NBAR data are ingested and used to compute the two band enhanced vegetation index (EVI2), along with ancillary data including VIIRS snow cover and land surface temperature (LST).
2. The background EVI2 value at each pixel (i.e., the minimum snow-free value) is identified and EVI2 values in the time series flagged as snow-contaminated are replaced with the background value. Details related to this procedure are provided in **Section 4**.
3. Data gaps associated with clouds and missing observations are filled using nonlinear interpolation (**Section 4**).
4. The time series of EVI2 data at each pixel are smoothed using a Savitzky-Golay filter and a running local median filter (**Section 4**).
5. To identify individual growth and senescence phases, time periods with sustained EVI2 increase and decrease are identified in the EVI2 time series at each pixel. To do this, a five-point moving slope technique is used, where transitions from periods of increasing

EVI2 to periods of decreasing EVI2 are identified by changes from positive to negative slope over five-point moving window, and vice versa. Because slight decreases or increases in EVI2 can be caused by local or transient processes unrelated to vegetation-growth cycles, two heuristics are applied to exclude such variation: (1) the change in EVI2 within any identified period of EVI2 increase or decrease must be larger than 20% of the annual range in EVI2 for the given pixel; and (2) the ratio of the local maximum EVI2 to the annual maximum EVI2 should be at least 0.25. This approach screens out short-term variation unrelated to growth and senescence cycles in a EVI2 time series, while at the same time allowing multiple growth cycles within any 12-month period to be identified.



6. Each vegetation growth cycle identified in the EVI2 data is modeled using a Hybrid Piecewise Logistic Model (HPLM) for each increasing and decreasing phase, separately. The HPLM accommodates EVI2 trajectories that are associated with both favorable conditions and stress conditions in vegetation growth using the following formulas (Figure 3):

$$EVI2(t) = \begin{cases} \frac{c_1}{1 + e^{a_1 + b_1 t}} + EVI2_b & \text{Favorable growth condition} & (1) \\ \frac{c_2 + dt}{1 + e^{a_2 + b_2 t}} + EVI2_b & \text{Vegetation stress condition} & (2) \end{cases}$$

where t is time in the day of year (DOY), a is related to the vegetation growth time, b is associated with the rate of plant leaf development, c is the amplitude of EVI2 variation, d is the vegetation stress factor, and $EVI2_b$ is the background value. In order to determine whether the plant suffers from stress or not, the time series fit to equations 1 and 2 are compared by using an index of agreement described in **Section 6**, and the function with

the best fit is used. The HPLM approach has several advantages: (1) it provides a simple, bounded, continuous function for modeling vegetation growth and decay processes; (2) each parameter can be assigned a biophysical meaning related to vegetation growth or senescence; (3) the algorithm is capable of describing either symmetric or asymmetric seasonal EVI2 dynamics; (4) it simulates multiple cycles of vegetation growths flexibly; and (5) the logistic model has been widely tested based on field measurements, webcam data, and remotely sensed data (e.g., Richards, 1959; Ratkowsky, 1983; Birch et al., 1998; Zhang et al., 2003; Richardson et al., 2006; Ahl et al., 2006), and it performs better than either the Fourier-based or asymmetric Gaussian functions for fitting remote sensing-based phenology development (Beck et al. 2006).

7. Phenological transition dates in each growth or senescence phase are identified using the rate of change in the curvature of the fitted HPLM models (Figure 3). Specifically, transition dates correspond to the day-of-year (DOY) on which the rate of change in curvature in the EVI2 data exhibits a local minima or maxima. These dates indicate when the annual cycle transitions from one approximately linear stage to another. Formally, at any time t , the curvature (K) for the HPLM given above is:

$$K = \frac{d\alpha}{ds} = \frac{EVI2''}{(1 + EVI2')^2} \quad (3)$$

where α is the angle (in radians) of the unit tangent vector at time t along a differential curve, s is the unit length of the curve, $EVI2'$ and $EVI2''$ are separately the first and second derivatives of equation 2. The curvature is small if the rate of change in EVI2 is relatively constant with time, and is large when the rate of change varies rapidly.

The curvature change rate (K') is the first derivative of the curvature K for the HPLM, which is the change in radians per unit length along the curve. During growth or senescence periods, when vegetation transitions from a dormant phase to a greenup up phase, or vice versa, three extreme points can be identified in the EVI2 curvature change rate (K'). During periods of increasing EVI2, the two maximum values correspond to the onset of EVI2 increase and the onset of EVI2 maximum, respectively (Figure 3). Transition dates indicating the onset of EVI2 decrease and EVI2 minimum during a senescence phase are estimated in a similar fashion.

8. For each cycle of vegetation growth and senescence, four phenological transition dates are recorded based on the day of year (DOY) when K' is at a maximum (during periods of EVI2 increase) and at a minimum (during periods of EVI2 decrease) (Figure 3). The corresponding phenological transition dates are defined as the onset of EVI2 increase (A), the onset of EVI2 maximum (C), the onset of EVI2 decrease (D), and the onset of EVI2 minimum (F). Day of year corresponding to the mid-point of greenup phase (B) and mid-point of senescent phase (E) are also identified. Based on these transition dates, the length of the vegetation growing season is also calculated (A-F). In addition, five EVI2 values for each growing cycle are estimated from the fitted HPLM curves: (1) the EVI2 at the onset of greenness increase (A'); (2) the EVI2 at the onset of greenness maximum (C'), (3) the sum of the daily EVI2 during the complete cycle, (4) the rate of change in EVI2 increase, and (5) the rate of change in EVI2 decrease.

9. Metrics characterizing VIIRS GLSP quality assurance and confidence in the phenology detections are recorded to provide information related to the overall confidence of the retrieved phenological metrics. This information is quantified using data quality information from the input EVI2 data set and HPLM model fit (**Section 6**).

4. Input Data and Preprocessing

4.1. Input data

To estimate global phenology, the VIIRS GLSP product algorithm requires 24 months of data for each 12-month period: the 12 months of interest, bracketed by six months on either side. Specific input data include 4 main parameters:

1. The daily VIIRS NBAR product (VNP43I) is used to calculate EVI2. EVI2 is calculated based on the same conceptual framework as the conventional EVI, but takes advantage of correlation between the red and blue wavelengths in surface reflectance spectra (Huete et al. 2006; Jiang et al. 2008) :

$$EVI2 = 2.5 \frac{\rho_{NIR} - \rho_{RED}}{\rho_{NIR} + 2.4\rho_{RED} + 1} \quad (1)$$

where ρ_{NIR} is reflectance in the near infrared waveband and ρ_{RED} is reflectance in the red waveband. To reduce data volumes while retaining fine temporal resolution, daily EVI2 values are aggregated to 3-day EVI2 composites by first selecting the best quality data within each 3-day window, and then using the maximum value composite method if more than one value remains. Similarly, corresponding NDVI values, along with quality flags from NBAR, are also recorded.

2. A snow and ice flag provided by the VIIRS snow product is also available in VIIRS NBAR quality flags. Using this flag, data points associated with snow-covered surfaces are removed from the input time series and replaced with snow-free “background EVI2” values (**Section 4.3**). This is important because the presence of snow introduces a large source of temporal variation in EVI2 that is not associated with vegetation phenology.
3. Land surface temperature (LST) obtained from VIIRS are used to screen periods where land surface temperature is too low to support vegetation growth and to determine background EVI2 (**Section 4.3**).
4. Land cover data is currently acquired from a static MODIS land cover product because a NASA VIIRS land cover product is currently not being produced. This dataset is used to determine whether the multiple cycles of vegetation growth are potentially possible for a specific land cover type. Specifically, forests are prescribed to have one growing cycle within a year, while croplands and grasslands can have multiple cycles. This rule helps characterize periods of relatively small EVI2 increases and decreases as artifacts or actual vegetation growth cycles. Moreover, land cover type is also used to estimate and prescribe the use of back-up EVI2 values (**Section 5.1**).

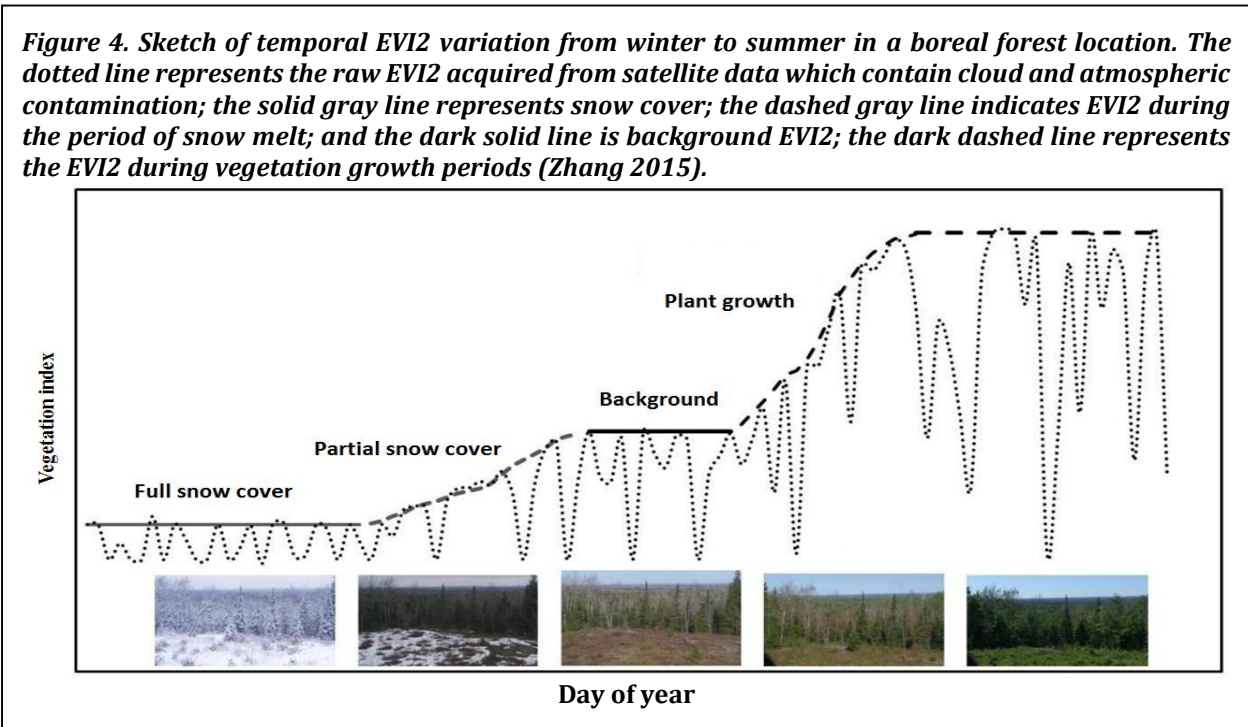
4.2. Smoothing and Gap Filling

Temporal smoothing of VIIRS EVI2 data is necessary because time series of EVI2 is generally noisy (Figure 4). The smoothing algorithm being used for the VIIRS GLSP product is based on four key assumptions:

1. Vegetation growth is a continuous process without sharp increases or decreases;
2. The time between successive peaks in separate vegetation growth cycles is longer than three months in forests and longer than two months for other plant functional types;
3. The magnitude of EVI2 values is lowered by contaminations from clouds, atmosphere, and snow cover; and
4. Local maxima in the EVI2 time series are not always reliable.

Persistent cloud cover is a major issue that significantly reduces the quality of EVI2 time series data. Globally, as much as 27% of the Earth's land surface is sufficiently obscured by clouds to prevent acquisition of good satellite data for consecutive 16 day period, and 16% of the surface is obscured for more than two months (Ju and Roy 2008; Zhang et al. 2006). While cloud cover is explicitly identified in the VIIRS NBAR data, residual unscreened cloud influences are still present in the current iteration of the data. Therefore, in the VIIRS GLSP, cloud-contaminated values in the EVI2 time series are detected by using the first three assumptions described above, and are filled using a moving average of two neighboring good quality values starting from the point close to the larger EVI2 values.

Unusually high EVI2 values can also arise from spuriously low red band values caused by incorrect atmospheric correction or a variety of other factors. To address this issue, all EVI2 values that are 90% larger than the corresponding NDVI, or EVI2 values that are 110%



larger than any EVI2 values within the previous and succeeding one month period, are replaced using good quality neighboring values. These thresholds have been identified based on comparison of NDVI and EVI2 time series across the globe.

After any cloud-contaminated values are replaced, Savitzky-Golay filters are applied to further reduce outliers in the EVI2 time series. Finally, a local median filter is applied to remove any remaining local outliers.

4.3. Snow-Contamination and Assignment of Background EVI2 Values

To account for the effect of snow on EVI2 data, the algorithm identifies the minimum snow-free EVI2 value (defined as the background EVI2, see Figure 4) for each pixel based on a two-year time series. The background EVI2 value represents the minimum EVI2 of the soil and vegetation mixture in an annual time series (Zhang 2015; Zhang et al. 2007). Assuming that vegetation is dormant during the winter (or with a cold surface with a daytime LST < 278K), the maximum EVI2 value during a dormant phase reflects the snow-free surface background condition before the onset of the growing season. However, reliable EVI2 values during winter are not always obtained from any given two-year periods that are also snow and cloud free. Thus, candidate background EVI2 values are determined using: (1) the mean of the 50% largest cloud and snow-free winter EVI2 values, where the winter period is determined based on LST values less than 278K, and (2) the mean of the 10% smallest cloud-free EVI2 values during periods where LST>278K occurs during the 2-year period of interest. The average of these two values is used as the background value if both cases are available. In the areas with widespread evergreen vegetation at low-latitudes or in areas that do not have sufficient good quality EVI2 during winter, the latter is selected. Note that the LST is used to identify irregular EVI2 values contaminated by snow or partial snow (including snow under the canopy) cover, instead of determining an exact winter period by date.

5. Related Technical Issues and Considerations

5.1. Back-Up EVI2 Values

The VIIRS GLSP algorithm often cannot provide reliable phenology detections for areas where the EVI2 values are consecutively missing due to cloud cover or other reasons. Indeed, cloud cover presents challenges in many parts of the tropics, sub-tropical monsoon climate regions, and some temperate and boreal zones.

To address these data gaps, the VIIRS GLSP approach employs a backup algorithm to fill the EVI2 values at pixels with consecutive missing values. For the VIIRS GLSP product, if the EVI2 values are consecutively missing for more than one month during the growing season, then EVI2 values with good quality in years directly preceding or following (if available) are first used to fill the missing observations in the year of interest. These cases are identified as ""processed, temporal backup algorithm" in the quality control (QC) field.

If the gap of missing EVI2 data is still larger than one month, after the above processing, the algorithm then uses available data from pixels in close proximity with the same land cover type. The final methodology for doing this requires knowledge of land cover and region-specific correlation length scales (i.e., to ensure the filling is done using statistically similar pixels). To distinguish between data from the main algorithm and gap-filled data,

quality assurance flags that explicitly identify values that have been filled using this strategy are included with the product. Specifically, this condition is referred to as "processed, spatial backup algorithm" in the QC field.

5.2. Limitations to Land Surface Phenology Retrievals

The VIIRS GLSP algorithm does not provide values where seasonal variation in EVI2 is low (e.g., arid and evergreen ecosystems). This leads to missing values in the product for pixels in almost all regions, but especially in arid and evergreen tropical ecosystems. Specifically, barren areas with no detectable phenology are identified as pixels where the annual amplitude is less than 0.02 EVI2 units. Evergreen systems are identified as pixels with maximum EVI2 greater than 0.6 and amplitude of variation in EVI2 less than 0.08. In these cases, we simply use "No processed, other" in the QC field.

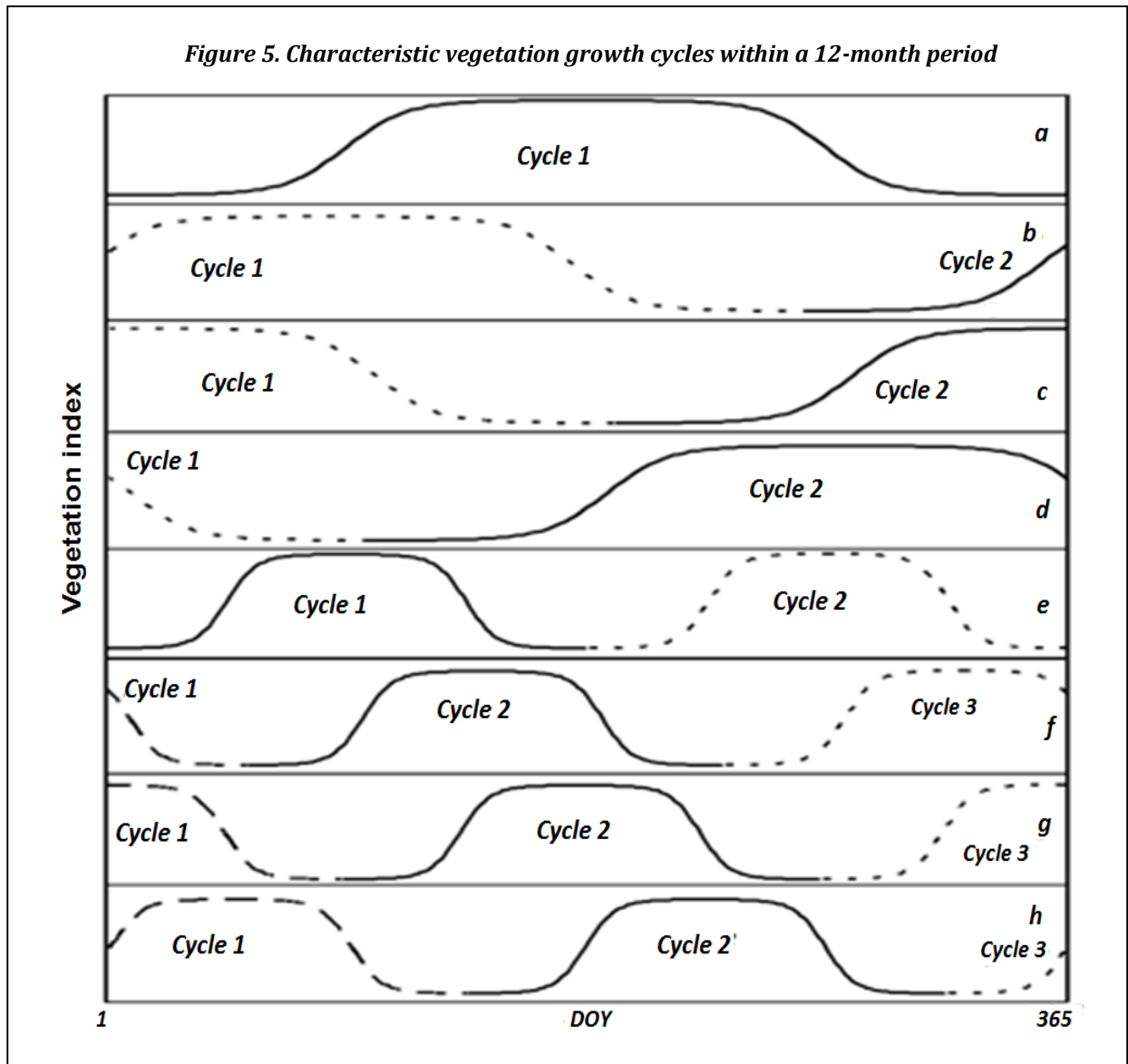
5.3. Geographic Variability in Growing Season Timing

The timing of growing seasons varies geographically, especially between the northern and southern hemispheres. Further, vegetation growth can have one or more cycles during a 12-month period. To account for both these properties, the algorithm used for this product allows for a maximum of two growth cycles in any given year.

To implement this feature, the product is provided with two "layers" corresponding to the first and second cycle (if present) at each pixel occurring during the period of interest. Further, depending on the location and period, a pixel may possess an incomplete cycle (truncated at the beginning or end). The combination of these factors introduces substantial complexity to the format in which these data are stored. Specific scenarios and examples are presented in Figure 5, and are discussed in the text that follows. Specifically, to allow for these different patterns, the algorithm is designed to accommodate four distinct scenarios:

1. Case (a) in Figure 5 presents the simplest scenario: a single, complete growth cycle centered near the mid-point of the 12-month period. In this case, the phenological metrics listed in Table 1 are recorded in the first layer of the product, and the second layer is populated entirely with fill values.
2. Cases (b), (c), and (d) illustrate situations in which two partial cycles are present during a 12-month period of interest. In these cases, the phenological parameters are recorded in layers 1 and 2, as appropriate, fill values are used for the phenological events that occur outside of the 12-month period, and the EVI2 area for both cycles is set equal to the fill value.
3. Case(e) illustrates the situation where two complete growth cycles are present and transition dates for each are provided in the two layers provided.
4. Cases (f), (g), and (h) illustrate examples where there are two incomplete cycles and one complete cycle. In this situation, only phenological metrics in the first two cycles are recorded. All parameters in the third cycle are recorded in the next period.

Note that the preceding or subsequent 12-month product period will capture the rest of the cycle for those cases with incomplete cycles (cases b, c, d, f, g, h).



6. VIIRS GLSP Quality Assurance

Quality assurance (QA) information is included as part of the VIIRS GLSP product. To this end, information related to the model fit and the proportion of high quality data used to estimate vegetation growth models is employed to quantify the relative quality of the LSP metrics at each pixel. The goal of this QA information is to characterize goodness of fit based on differences between the modeled values and satellite measurements at each pixel. A variety of metrics can be used for this purpose (e.g., root mean squared error (RMSE), the coefficient of determination, or residual standard deviation); however, these parameters are not comparable across different biomes and climate regimes. For example, because the magnitude of EVI2 values is higher over humid regions, model RMSEs tend to be larger in forests than that in shrublands, even though the models perform much better in forests.

Moreover, the coefficient of determination can be strongly influenced by a few extreme samples. To address this, we use an index of model agreement (Willmott 1981; Zhang 2015):

$$AI = 100 - 100 \frac{\sum_{i=1}^n \left(P(i) - O(i) \right)^2}{\sum_{i=1}^n \left(\left| P(i) - \bar{O} \right| + \left| O(i) - \bar{O} \right| \right)^2} \quad (3)$$

where n is the number of observations with good (or better) quality (note: input data with lower quality are not used to fit the model), $P(i)$ is the fitted value, $O(i)$ is the observation, and \bar{O} is the mean observed value. Thus, the AI value provides a measure of relative error in model estimates at each pixel. It is dimensionless and ranges from 0 to 100, where 0 describes complete disagreement between estimated and observed values, and 100 indicates that the estimated and observed values are identical. It is also sensitive to differences between observed and estimated means (Willmott, 1981), and therefore provides a goodness of fit measure that is comparable across biomes.

Because the quality of the fitted model at each pixel is strongly dependent on the number of good quality observations during the vegetation growing season (Zhang et al. 2009), the proportion of good quality (P_{gq}) EVI2 values for a given pixel is also included in the quality assurance data for that pixel. Based on sensitivity analysis, error in vegetation phenology detection using logistic models is at a minimum if the temporal resolution of the vegetation index is finer than 8 days (Zhang et al. 2009). In other words, vegetation temporal trajectories can be realistically reconstructed if there is a good EVI2 observation within each 8-day period during the growing season. For the VIIRS GLSP we are using 3-day inputs, and the P_{gq} during each growing season at each pixel is calculated as:

$$P_{gq} = \frac{N_{gq}}{T} \times 100 \quad (4)$$

where P_{gq} is the proportion of good quality observations (ranging from 0 to 100), T is the total number of 3-day EVI2 during a growing season, and N_{gq} is the number of three 3-day moving windows that contain good quality observations.

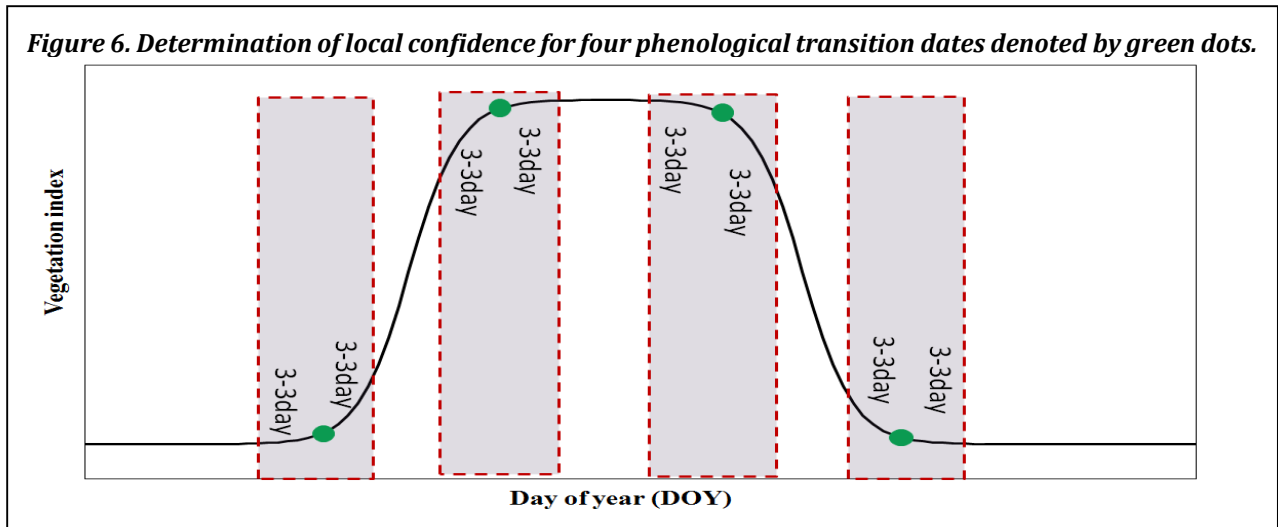
To generate an aggregate QA score based on both the AI and P_{gq} at each pixel during each growth cycle, the proportion of good quality data and the index of agreement, both of which scale from 0 to 100, are fused to produce the overall measure of confidence. Specifically, the overall quality assurance (QA) of phenological detections in the VIIRS GLSP product is defined as:

- QA=0 (processed, good quality), if $P_{gq} \geq 60$ and $AI \geq 60$
- QA=1 (processed, other quality), if $20 \leq P_{gq} < 60$ or if $AI < 60$ and $P_{gq} \geq 20$
- QA=2 (processed, backup algorithm), if the length of consecutive missing EVI2 >30 days
- QA=3 (not processed, bad quality), if $P_{gq} < 20\%$
- QA=4 (not processed, other), if the growing season amplitude in EVI2 < 0.08 in forests and EVI2 < 0.02 in other ecosystems

Further, as we mentioned earlier, the four key phenological dates are the most important metrics in the product. To fully provide a confidence metric for each phenological date included

in the VIIRS GLSP product, local EVI2 quality around each transition date is used to describe the confidence in the corresponding phenological detection. Specifically, the local confidence for each transition date metric is defined as the proportion of good EVI2 values during the three 3-day periods before and after the detected phenological timing (Figure 6). This time period was determined based on a previous sensitivity analysis of phenology date detections (Zhang et al. 2009). Note that a low local confidence does not necessarily indicate that the detected phenological timing is incorrect, just that the uncertainty associated with the estimated date is high.

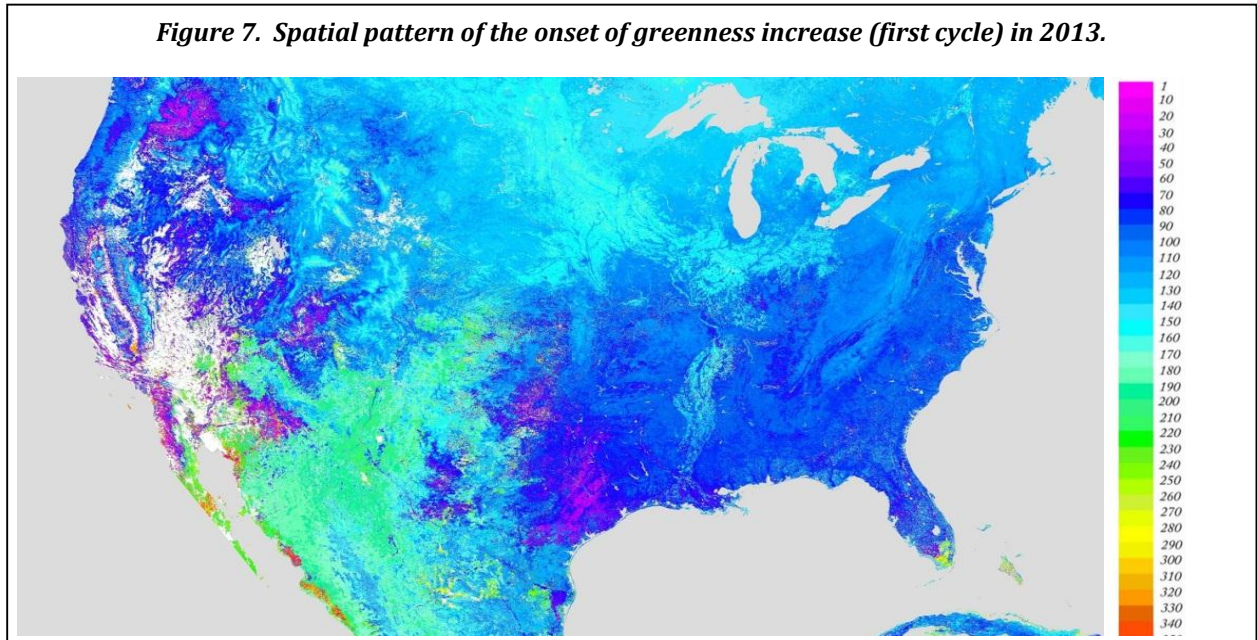
Figure 6. Determination of local confidence for four phenological transition dates denoted by green dots.



7. Product Implementation and Initial Accuracy Assessment

This section includes two elements. First, we present results from the VIIRS GLSP in North America in 2013 and 2014. Second, we discuss the evaluation of VIIRS GLSP. Note that the VIIRS reflectance algorithms were still being revised and that the input data were not

Figure 7. Spatial pattern of the onset of greenness increase (first cycle) in 2013.



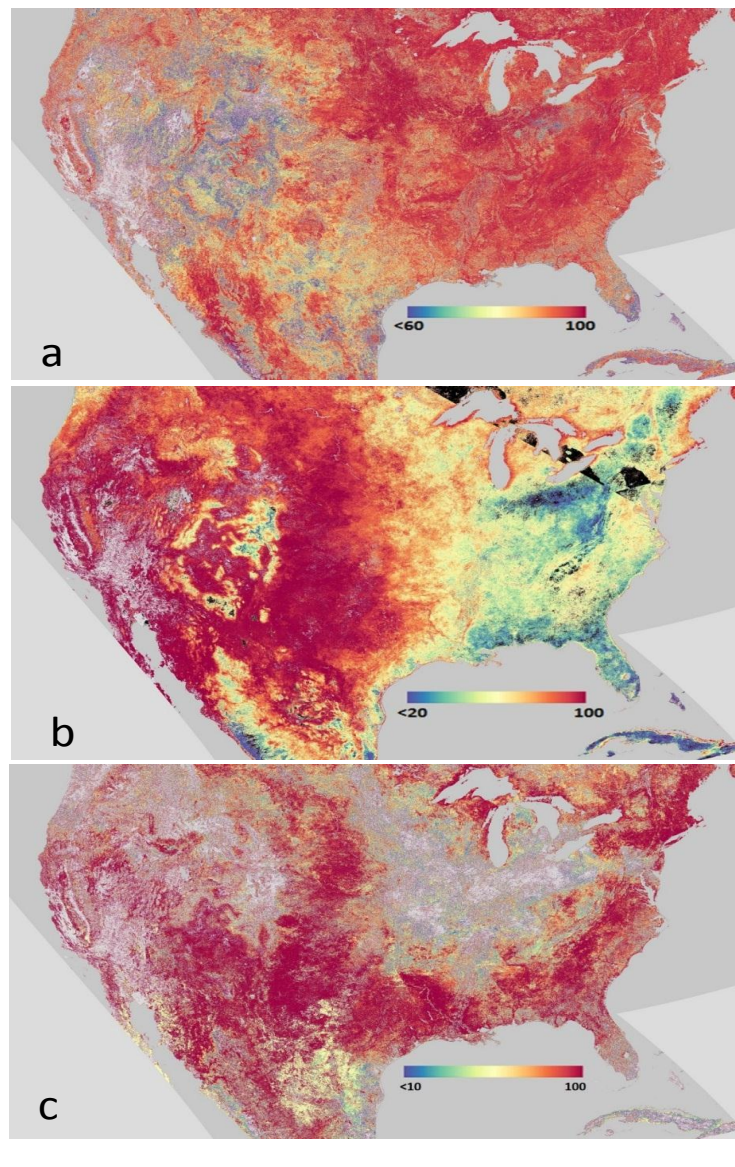
stable when these results were generated. We anticipate test results will improve modestly when the final updated VIIRS NBAR and LST products are available.

7.1. VIIRS GLSP algorithm Results in North America

The VIIRS GLSP algorithm was tested using 500m spatial resolution using daily VIIRS NBAR time series observations from July 2012 to June 2015. We obtained 14 tiles of these data from the VIIRS NBAR VNP43I4 product developer (collaborator Crystal Schaaf, University of Massachusetts Boston) because the official VIIRS NBAR products were not yet available when we generated these results. These tiles (H08V04, H08V05, H08V06, H09V04, H09V05, H09V06, H10V04, H10V05, H10V06, H11V04, H11V05, H12V04, H12V05 and H13V04) cover the entire Contiguous United States (CONUS), southern Canada, and northern Mexico. Land surface temperature and land cover were acquired from the MODIS products (MYD11, MCD12).

Figure 7 shows the spatial pattern in the day of year corresponding to the onset of greenness increase in 2013. In the eastern regions, greenup started in late February in the south, and shifted northwards gradually. Greenup onset occurs 10-20 days later than surrounding natural vegetation in the croplands of the mid-west and the Mississippi valley. In western regions, the geo-graphic patterns in the timing of greenup onset are complex and do not show an obvious latitudinal gradient. Greenup starts during June and July in the southwest, where monsoon precipitation

Figure 8. Confidence of VIIRS GLSP detection in 2013. (a) confidence in the index of model agreement (AI), (b) confidence in the proportion of good quality observations (P_{gq}), (c) local confidence in greenup onset. The light gray inside the land area represents confidence "0" or no phenology detection while outside the land indicates out of the selected VIIRS tiles. Back color in (b) indicates no good VIIRS observations for more than consecutive one month (including cloud cover and other impacts).



drives vegetation seasonality. Two cycles of vegetation growth are also evident locally in areas such as Texas, where the first growing cycle starts in late January, followed by a second cycle in late August. Other phenological transition dates show similar spatial patterns.

Figure 8 shows maps of the confidences associated with the VIIRS GLSP detections. The agreement index for the HPLM model was very high in much of the central and eastern CONUS, and was generally larger than 90%, in regions where forests and croplands are dominant (Figure 8a). In the western areas, the agreement index was substantially lower, because shrublands and savannas are the major vegetation cover, and vegetation seasonality cannot always be detected in these land covers due to a low amplitude in the seasonality of EVI2 time series, and in some years, because of drought affecting these land covers.

The proportion of good VIIRS observations show spatial patterns that are different from those exhibited by the agreement index (Figure 8b). In the eastern areas, cloud contamination is much more frequent than in the western region, leading to lower values of P_{gq} . Note that black pixels reflect large proportions of missing VIIRS EVI2, which are likely associated with instrument problems or problems with upstream data processing.

Finally, local confidence values associated with individual phenological transition dates reflect variability in the quality of the VIIRS input data. This is demonstrated in the local confidence values assigned to the timing of the EVI2 increase onset (Figure 8c). In both the mid-western and northwestern US, frequent cloud cover reduced the detection accuracy of the spring greenup onset.

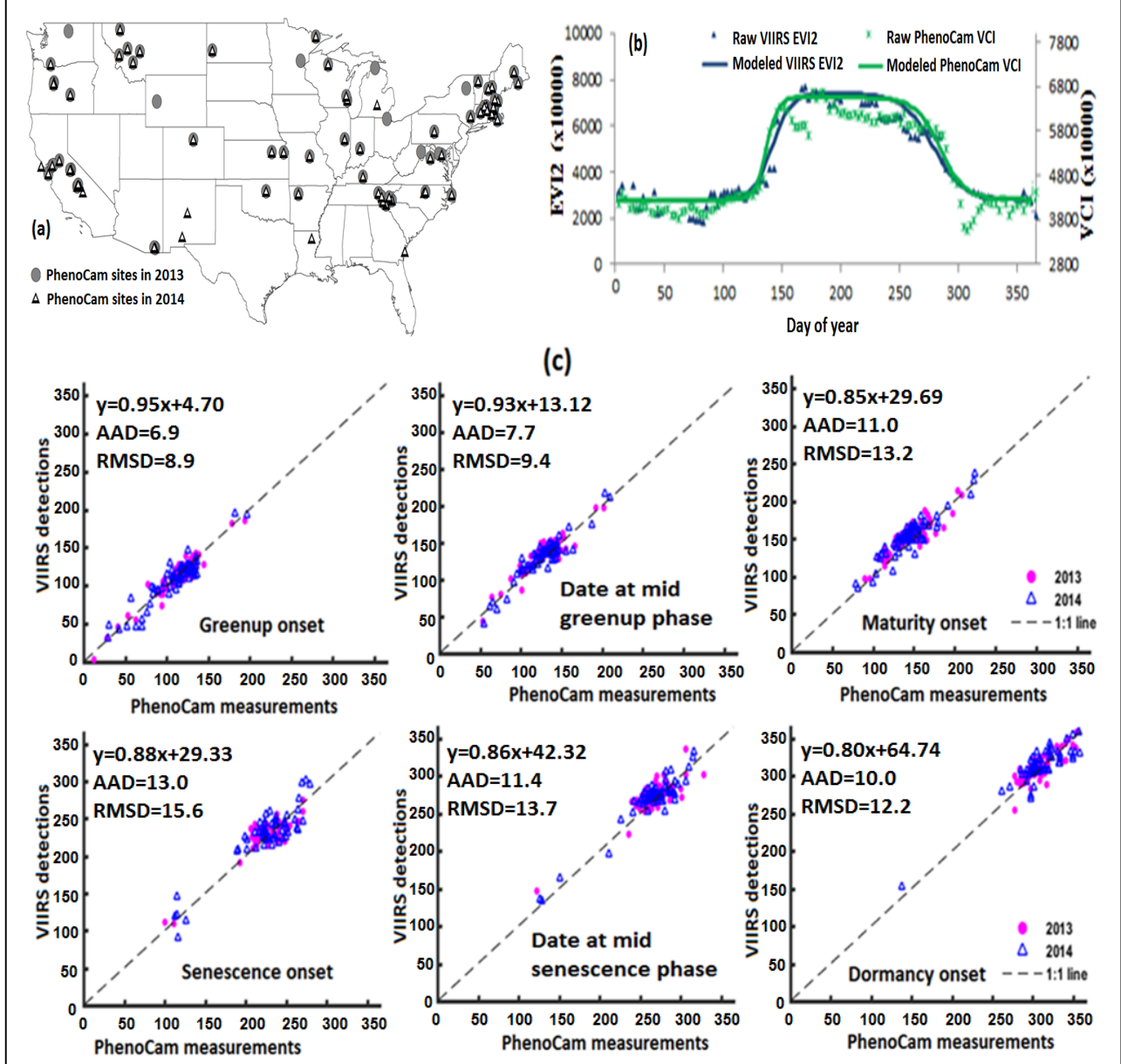
7.2. Evaluation of VIIRS GLSP

Robust characterization of error and uncertainty in land surface phenology metrics is a critical requirement and goal of the VIIRS GLSP product. However, validation of land surface phenology is very challenging. In-situ measurements of phenology are rare, and where available, are often based on citizen scientist observations of individual plants or species collected at scales well below the spatial resolution of the VIIRS product. These data are therefore difficult to compare with satellite-based measurements of land surface phenology. For example, we have previously exploited data sets collected by staff at the Harvard Forest and Hubbard Brook LTER (Long Term Ecological Research) sites for the evaluation of MODIS Land Cover Dynamics product (Ganguly et al. 2010; Zhang et al. 2006). However, these data are representative of a fairly narrow ecological zone (northeastern hardwood forests) and are collected using different methods and metrics that are not designed for comparison with satellite-derived measures of land surface phenology. We have also previously quantified errors associated with different vegetation index compositing periods and methods (Zhang et al., 2009). For the VIIRS GLSP, we are evaluating product accuracy using two sources of assessment data that more directly complement the nature and scale of VIIRS measurements. Specifically, we are using data from the so-called “PhenoCams” and data based on retrievals of land surface phenology from dense time series of Landsat data (e.g., Melaas et al., 2013).

PhenoCam observations have become a valuable tool for evaluating and understanding satellite-derived land surface phenology because they provide consistent and continuous measurements of canopy-scale vegetation canopy conditions (Hufkens et al. 2012; Richardson et al. 2009a; Richardson et al. 2007; Sonnentag et al. 2012). The PhenoCam network currently includes over 300 cameras that provide over roughly 600 site years of

data distributed across North America (<http://klima.sr.unh.edu/>). Analysis of PhenoCam data relatively early in the PhenoCam project, provided proof-of-concept demonstrations regarding the utility of the PhenoCam products for assessing land surface phenology results (Klosterman et al. 2014). The weakness of PhenoCams for assessment of the VIIRS GLSP is that they use primarily visible color bands, which are not equivalent to satellite vegetation indices derived from red and near infrared reflectances (although more and more of the PhenoCams are now including NIR information as well). Moreover, the mismatch in the camera's oblique view angle with the satellite pixel view angle introduces substantial uncertainty in comparisons of PhenoCam time series to satellite VI time series (Elmore et al.

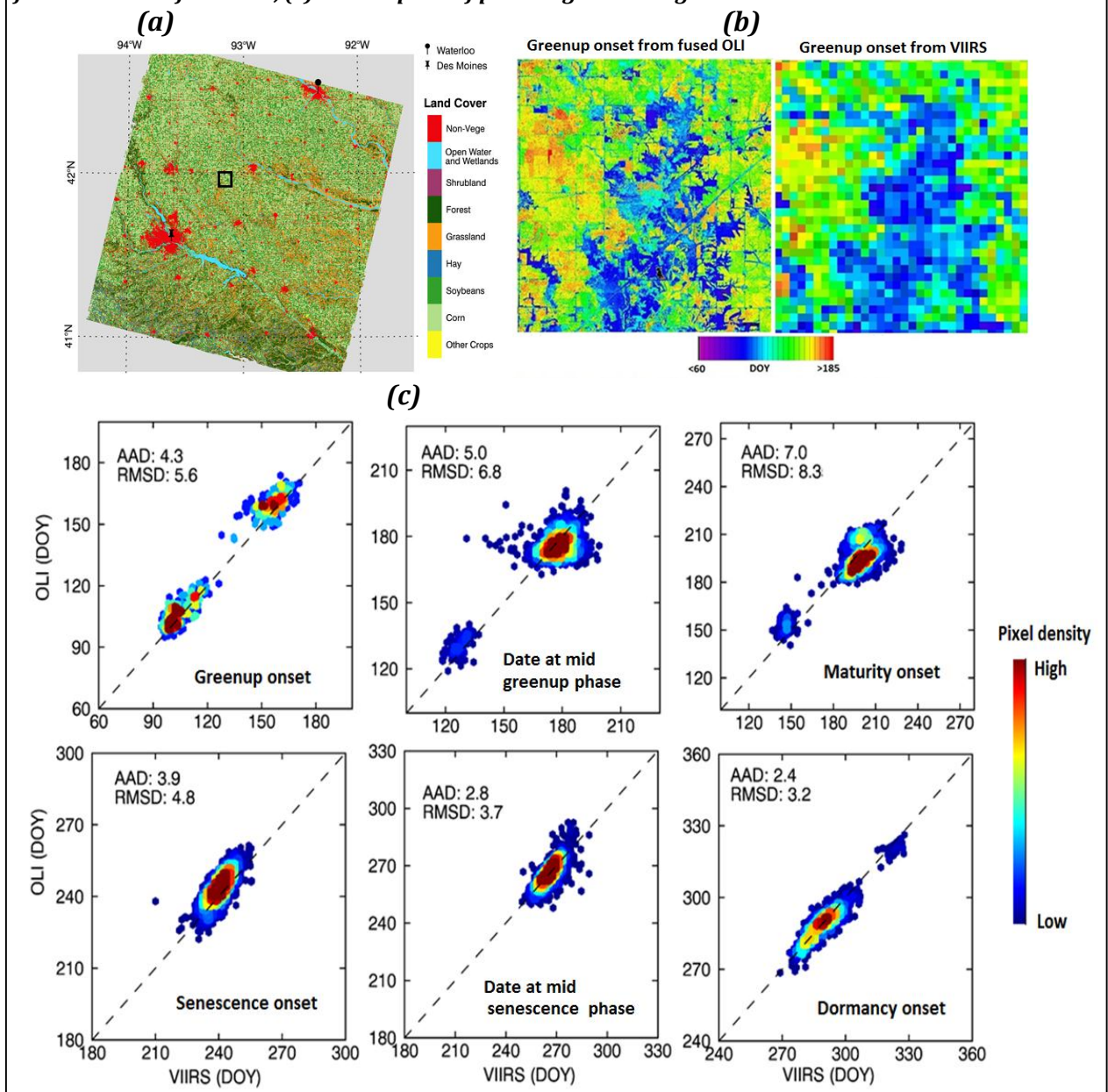
Figure 9. Comparison between VIIRS GLSP and PhenoCam measurements. (a) PhenoCam sites, (b) VIIRS EVI2 and PhenoCam VCI in the Harvard Forest site, (c) scatter plots of phenological timing between VIIRS EVI2 detections and PhenoCam measurements.



2012; Graham et al. 2010; Hufkens et al. 2012; Keenan et al. 2014a). This is exacerbated by the difference in the field-of-view of the two products.

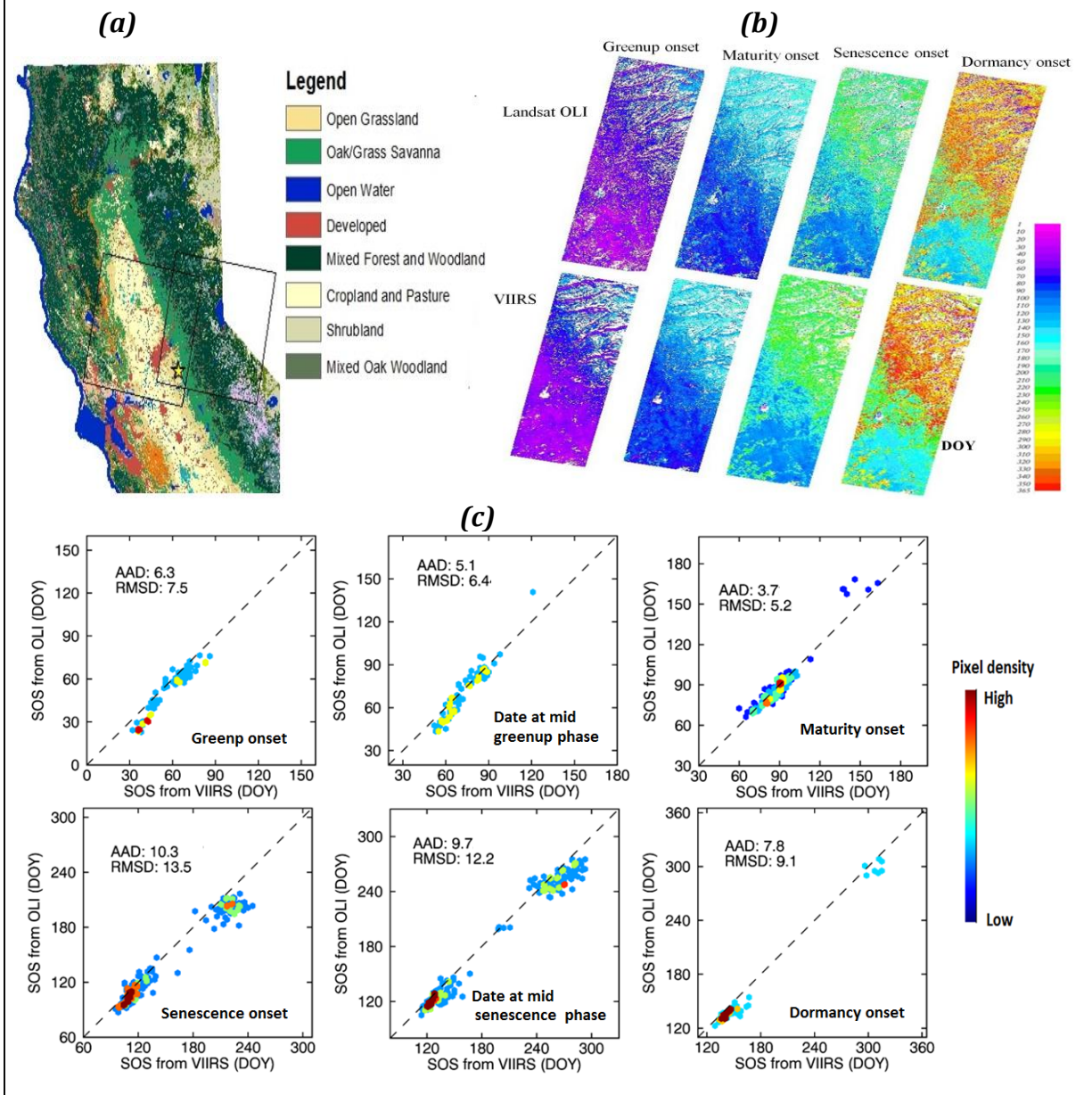
Despite these limitations, the PhenoCam archive represents one of the best available datasets for evaluating land surface phenology. To provide an initial assessment of VIIRS GLSP, we compiled PhenoCam data from across the CONUS in 2013 and 2014, which span a wide range of ecosystem and climate conditions and therefore provide a useful basis for VIIRS GLSP product assessment (Figure 9). To perform this assessment, daily vegetation contrast index (VCI) values were calculated using DN values from the red (R), green (G), and

Figure 10. Comparison of phenological detections from VIIRS NBAR EVI2 (500m) and fused MODIS-Landsat OLI data (30m) in 2013 in the central US (subset of Landsat scene path 26 and row 31). (a) Land cover types in the comparison area, (b) enlarged local area (black box in a) for timing of greenup onset from VIIRS and fused OLI, (c) scatter plots of phenological timing between VIIRS and OLI measurements.



blue (B) color channels [$VCI=G/(R+B)$] in PhenoCam imagery. Phenological transition dates were then identified from the VCI time series using the VIIRS HPLM algorithm. Preliminary results comparing the transition dates estimated from the VIIRS EVI2 time series to those obtained from the PhenoCam VCI time series indicate that the VIIRS GLSP detections are very similar to the observations from PhenoCam, although the differences are somewhat larger in autumn than in the spring (Figure 9). The average absolute difference (AAD) is 7 days and the root mean square difference (RMSD) is 9 days for the timing of greenness onset, and about

Figure 11. Comparison of phenological detections from VIIRS NBAR EVI2 and Landsat OLI data in 2014 in the Sierra Nevada Mountains, California. (a) Land cover types, (b) spatial pattern of phenological metrics from OLI (30m) and VIIRS (500m), and (c) comparison between VIIRS GLSP and OLI phenology in relatively homogeneous areas.



11 days for the timing of dormancy onset. As expected, the largest differences were associated with the timing of senescence onset.

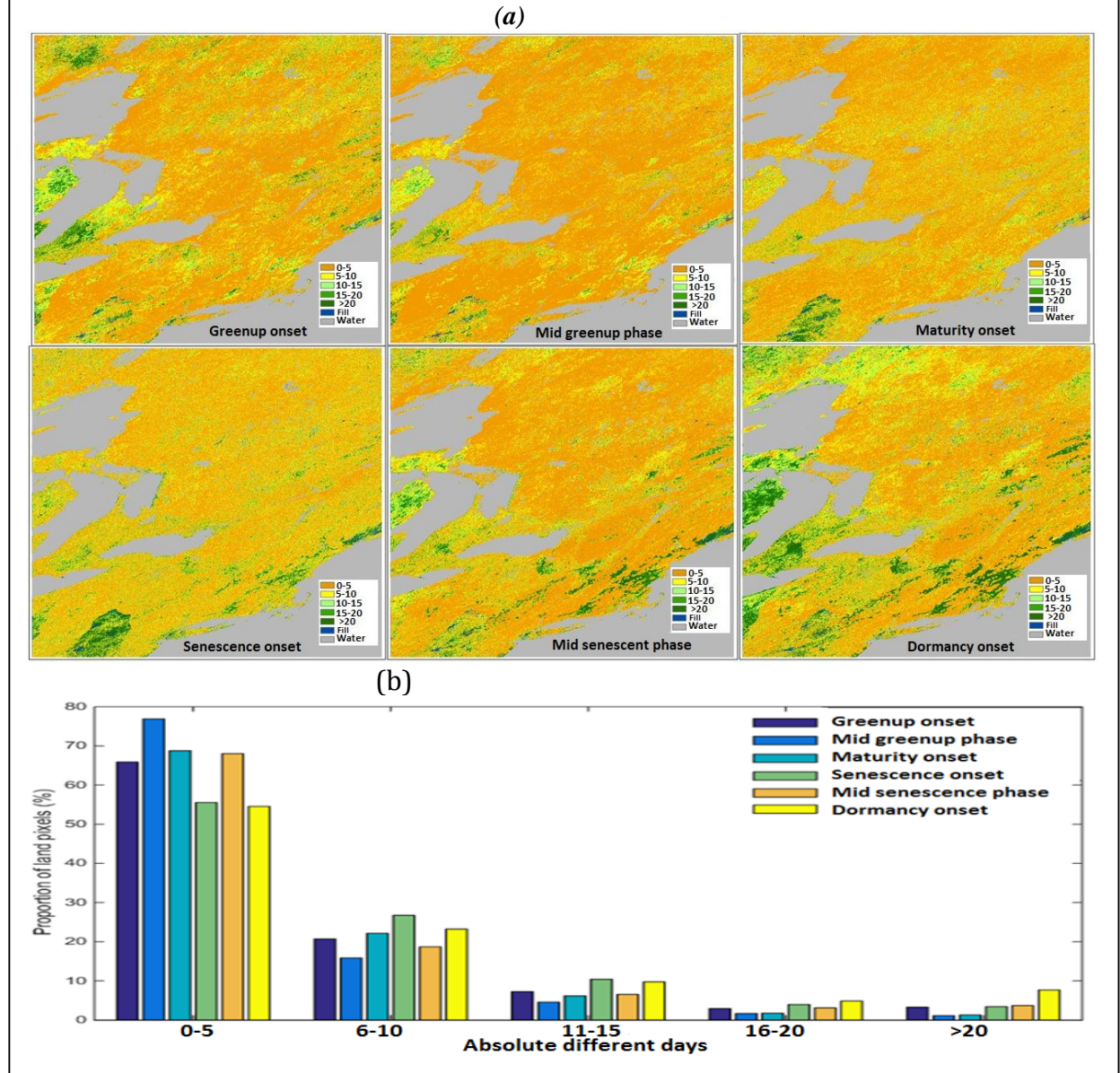
In addition to PhenoCam, the deep and growing archive of cloud-free Landsat data offers another independent source of phenological observations for the assessment of the VIIRS GLSP product. The Landsat Thematic Mapper family of sensors offers an atmospherically corrected multispectral nadir view to complement the RGB oblique view of the PhenoCams. These data are also freely accessible through Web Enabled Landsat Data (WELD) product (<http://weld.cr.usgs.gov>) (Roy *et al.*, 2010). In addition, Landsat 8 Operational Land Imager (OLI) data have been available since February 2013. Although the temporal frequency of Landsat data is relatively poor for monitoring land surface phenology development, fused time series from Landsat and daily MODIS data can provide observations with high temporal and spatial resolution (Gao *et al.* 2006), which can then be used to measure field scale phenology and to evaluate the VIIRS GLSP (Gao *et al.* 2017). To this end, we estimated Landsat-scale phenological metrics from daily fused MODIS - Landsat8 OLI (path 26 and row 31 in the central US) reflectances (30m) in 2013 and 2014, and compared these data to VIIRS GLSP detections at 500m (Figure 10). The results indicate that differences in homogeneous regions were much smaller than in regions with heterogeneous land cover, and that the overall AAD for the onset of greenness increase was less than 5 days. Furthermore, in ~20% of the relatively homogeneous pixels, the AAD was less than 5 days for the all transition dates except for maximum EVI onset, and the RMSD was less than 8 days for all six phenological timing metrics (Figure 10).

Another source of evaluation data that does not require fusing Landsat data with MODIS is to exploit the denser time series of available in so-called sidelap zones between adjacent Landsat scenes. We used this approach to evaluate the VIIRS GLSP semiarid environments, where land surface phenology is very complex because the phenological timing of grasses is not synchronous with overstory trees. In Figure 11, we show results for the Landsat 8 OLI imagery in the sidelap zone between path 43/row 33 and path 44/row 33 (the Sierra Nevada Mountains, California) in 2013 and 2014. Results from this comparison indicate that the six VIIRS GLSP phenological dates (500m) were all comparable to those estimated from Landsat OLI, with most ADD values less than 10 days and RMSD less than 14 days in 20% of the most homogeneous pixels (Figure 11). As for the comparison with PhenoCam results, differences in the vegetation greenup phase were much smaller than those in the senescence phase.

In a final comparison, the VIIRS GLSP was compared with the MODIS Land Cover Dynamics Product (MCD12Q2) to provide a baseline understanding of the continuity between these two long-term GLSP products. MCD12Q2 results are estimated using the MODIS NBAR product (MCD43A4) which is produced from a combination of Terra MODIS and Aqua MODIS. Hence, MODIS NBAR time series have more cloud free observations than VIIRS NBAR time series. With this in mind, we calculated absolute difference of phenological dates between VIIRS GLSP and MODIS GLSP in New England tiles (H12V04) after applying a 3 by 3 smoothing window to both data sets. The smoothing is used to reduce some of the uncertainties brought about by the effective spatial resolution difference as the actual size of a 500m gridded VIIRS pixel represents a median effective resolution of 565m by 595m, while a 500m gridded MODIS pixel represent a median effective resolution of 833m by 618m (Campagnolo *et al.* 2016). The results indicate that the differences between these two products were less than 5 days and 10 days in more than

55% and 80% of pixels, respectively (Figure 12). Areas with differences larger than 20 days were generally associated with missing observations in VIIRS time series.

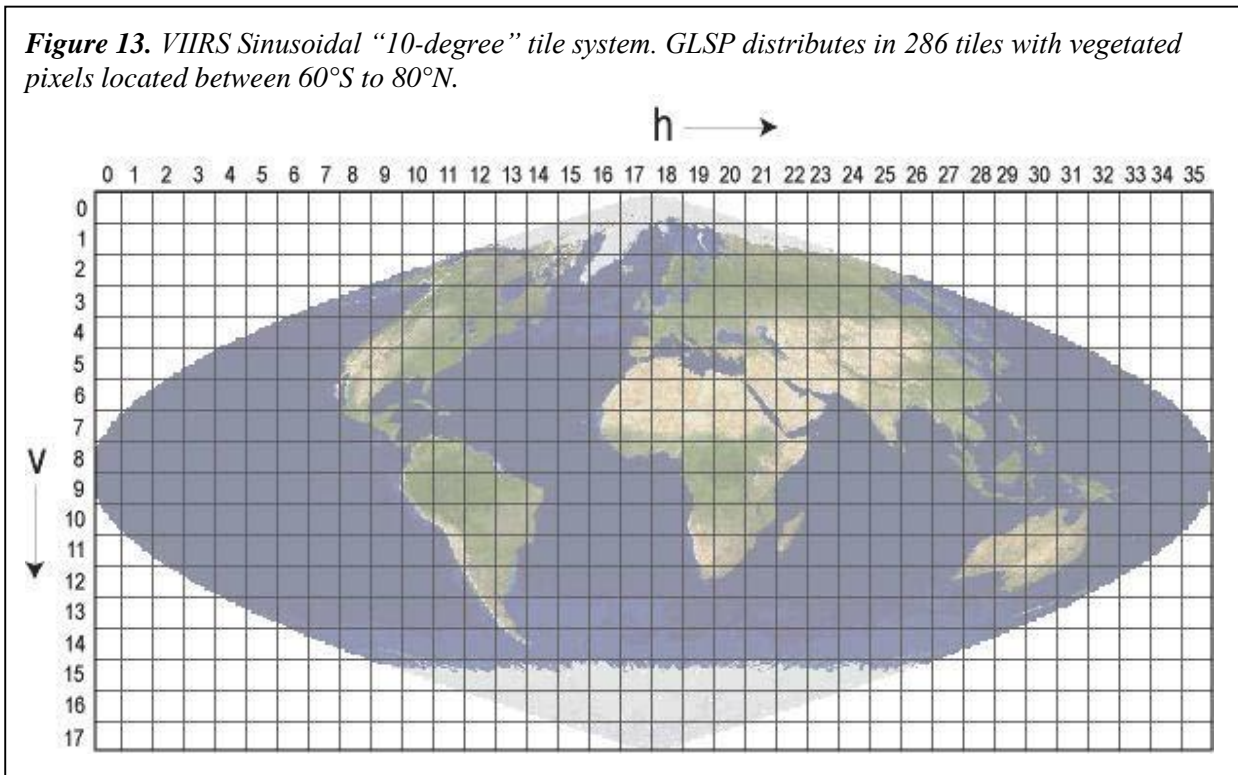
Figure 12. Absolute timing differences for phenological metrics from VIIRS and MODIS over northeastern CONUS in 2013. (a) Spatial pattern and (b) proportion of pixels in six phenological metrics.



8. Land Surface Phenology Specification

VIIRS GLSP product is a level 4 product and follows the structure and file format used in high level of global VIIRS data. The data are saved in HDF5 (Hierarchical Data Format - Earth Observing System) file format in a Sinusoidal map projection. Since the VIIRS GLSP is detected

for vegetated land surface, only 286 tiles are produced because other tiles are either water or have no vegetated pixels (Figure 13). Each tile covers 10-degree from 60°S to 80°N.



8.1. Science Data Records

The VIIRS Land Surface Phenology product includes eleven Science Data Sets (SDS) for each pixel. The longnames and formats of these SDSs are:

DataField	Name	Format
DataField_1	Onset_Greenness_Increase	UINT16
DataField_2	Onset_Greenness_Maximum	UINT16
DataField_3	Onset_Greenness_Decrease	UINT16
DataField_4	Onset_Greenness_Minimum	UINT16
DataField_5	Date_Mid_Greenup_Phase	UINT16
DataField_6	Date_Mid_Senescence_Phase	UINT16
DataField_7	Growing_Season_Length	UINT16
DataField_8	EVI2_Onset_Greenness_Increase	UINT16
DataField_9	EVI2_Onset_Greenness_Maximum	UINT16
DataField_10	EVI2_Growing_Season_Area	UINT16
DataField_11	Rate_Greenness_Increase	UINT16
DataField_12	Rate_Greenness_Decrease	UINT16
DataField_13	Greenness_Agreement_Growing_Season	UINT8

DataField_14	PGQ_Growing_Season	UINT8
DataField_15	PGQ_Onset_Greenness_Increase	UINT8
DataField_16	PGQ_Onset_Greenness_Maximum	UINT8
DataField_17	PGQ_Onset_Greenness_Decrease	UINT8
DataField_18	PGQ_Onset_Greenness_Minimum	UINT8
DataField_19	GLSP_QC	UINT8

Each DataField (except DataField_13) includes two 16-bit (UINT16) values, one for each of two possible growth cycles in the 12-month period included. Missing data due to clouds or absence of detectable phenology will be given a value of 32767. DataField_13 includes six 8-bit (UINT8) values and fill value is 255.

8.2. Product Specification

The product is distributed in the standard land Hierarchical Data Format (HDF5), and includes the following data layers, defining for each 500m pixel:

Onset_Greenness_Increase: UINT16

 Description: Days starting from January 1, 2000

 Data conversions:

 DOY=file data - (given year-2000)*366

 Cycle: Word 1 is first mode of the year and word 2
 is second mode of the year (other possible
 modes are not reported)

 Fill_Value: 32767

 Units: Day

 Valid Range: 1-32766

Onset_Greenness_Maximum: UINT16

 Description: Days starting from January 1, 2000

 Data conversions:

 DOY=file data - (given year-2000)*366

 Cycle: Word 1 is first mode of the year and word 2
 is second mode of the year (other possible
 modes are not reported)

 Fill_Value: 32767

 Units: Day

 Valid Range: 1-32766

Onset_Greenness_Decrease: UINT16

 Description: Days starting from January 1, 2000

 Data conversions:

 DOY=file data - (given year-2000)*366

 Cycle: Word 1 is first Mode of the year and word 2
 is second mode of the year (other possible
 modes are not reported)

Fill_Value: 32767
 Units: Day
 Valid Range: 1-32766

Onset_Greenness_Minimum: UINT16
 Description: Days starting from January 1, 2000
 Data conversions:
 DOY=file data - (given year-2000)*366
 Cycle: Word 1 is first Mode of the year and word 2
 is second mode of the year (other possible
 modes are not reported)
 Fill_Value: 32767
 Units: Day
 Valid Range: 1-32766

Date_Mid_Greenup_Phase: UINT16
 Description: Days starting from January 1, 2000
 Data conversions:
 DOY=file data - (given year-2000)*366
 Cycle: Word 1 is first mode of the year and word 2
 is second mode of the year (other possible
 modes are not reported)
 Fill_Value: 32767
 Units: Day
 Valid Range: 1-32766

Date_Mid_Greenup_Phase: UINT16
 Description: Days starting from January 1, 2000
 Data conversions:
 DOY=file data - (given year-2000)*366
 Cycle: Word 1 is first mode of the year and word 2
 is second mode of the year (other possible
 modes are not reported)
 Fill_Value: 32767
 Units: Day
 Valid Range: 1-32766

Growing_Season_Length: UINT16
 Description: Number of days in a growing cycle
 Data conversions:
 Day=file data
 Cycle: Word 1 is first Mode of the year and word 2
 is second mode of the year (other possible
 modes are not reported)
 Fill_Value: 32767
 Units: Number of days

Valid Range: 1-366

EVI2_Onset_Greenness_Increase: UINT16

Description: EVI2 value at onset of greenness increase during a growth cycle

Data conversions:

$EVI2 = \text{file data} * 0.0001$

Cycle: Word 1 is first Mode of the year and word 2
is second mode of the year (other possible
modes are not reported)

Fill_Value: 32767

Valid Range: 1-10000

EVI2_Onset_Greenness_Maximum: UINT16

Description: EVI2 value at onset of greenness maximum during a growth cycle

Data conversions:

$EVI2 = \text{file data} * 0.0001$

Cycle: Word 1 is first Mode of the year and word 2
is second mode of the year (other possible
modes are not reported)

Fill_Value: 32767

Valid Range: 1-10000

EVI2_Growing_Season_Area: UINT16

Description: EVI2 area under curve in a growing cycle

Data conversions:

$EVI2 = \text{file data} * 0.01$

Cycle: Word 1 is first Mode of the year and word 2
is second mode of the year (other possible
modes are not reported)

Fill_Value: 32767

Valid Range: 1-32766

Rate_Greenness_Increase: UINT16

Description: Average rate of EVI2 increase during a greenup phase

Data conversions:

$EVI2/\text{day} = \text{file data} * 0.0001$

Cycle: Word 1 is first Mode of the year and word 2
is second mode of the year (other possible
modes are not reported)

Fill_Value: 32767

Units: EVI2 per day

Valid Range: 1-32766

Rate_Greenness_Decrease: UINT16

Description: Average rate of VI decrease during a senescent phase

Data conversions:

EVI2/day=file data*0.0001
 Cycle: Word 1 is first Mode of the year and word 2
 is second mode of the year (other possible
 modes are not reported)

Fill_Value: 32767
 Units: EVI2 per day
 Valid Range: 1-32766

Greenness_Agreement_Growing_Season: UINT8
 Description: An index of model agreement between modeled EVI2 values and
 satellite measurements (good quality) during a growing season (0-100)
 Cycle: Word 1 is first Mode of the year and word 2 is second mode of the year (other
 possible modes are not reported)
 Fill_Value: 255
 Units: Dimensionless
 Valid Range: 1-100

PGQ_Growing_Season: UINT8
 Description: Proportion of good quality VIIRS observations during a growing season
 (0-100)
 Cycle: Word 1 is first Mode of the year and word 2 is second mode of the year (other
 possible modes are not reported)
 Fill_Value: 255
 Units: Dimensionless
 Valid Range: 1-100

PGQ_Onset_Greenness_Increase: UINT8
 Description: Proportion of good quality VIIRS observations around the onset of
 greenness increase (0-100)
 Cycle: Word 1 is first Mode of the year and word 2 is second mode of the year (other
 possible modes are not reported)
 Fill_Value: 255
 Units: Dimensionless
 Valid Range: 1-100

PGQ_Onset_Greenness_Maximum: UINT8
 Description: Proportion of good quality VIIRS observations around the onset of
 greenness maximum (0-100)
 Cycle: Word 1 is first Mode of the year and word 2 is second mode of the year (other
 possible modes are not reported)
 Fill_Value: 255
 Units: Dimensionless
 Valid Range: 1-100

PGQ_Onset_Greenness_Decrease: UINT8

Description: Proportion of good quality VIIRS observations around the onset of greenness decrease (0-100)

Cycle: Word 1 is first Mode of the year and word 2 is second mode of the year (other possible modes are not reported)

Fill_Value: 255

Units: Dimensionless

Valid Range: 1-100

PGQ_Onset_Greenness_Minimum: UINT8

Description: Proportion of good quality VIIRS observations around the onset of greenness minimum (0-100)

Cycle: Word 1 is first Mode of the year and word 2 is second mode of the year (other possible modes are not reported)

Fill_Value: 255

Units: Dimensionless

Valid Range: 1-100

GLSP_QC: UINT16

Description: Quality flags for vegetation phenology

Note: First Word:

the first three (0-2) bits are Mandatory QA

0=processed, good quality

1=processed, other quality

2=processed, backup algorithm

3=not processed, bad quality

4=not processed, other

the next two (3-4) bits are TBD

the 5-7 bits are Land Water mask

(as passed down from NBAR

0 = Shallow ocean

1 = Land (Nothing else but land)

2 = Ocean coastlines and lake shorelines

3 = Shallow inland water

4 = Ephemeral water

5 = Deep inland water

6 = Moderate or continental ocean

7 = Deep ocean

Fill_Value: 255

Units: Dimensionless

Valid Range: 1-100

9. Literature Cited

- Angert, A., Biraud, S., Bonfils, C., Henning, C.C., Buermann, W., Pinzon, J., Tucker, C.J., & Fung, I. (2005). Drier summers cancel out the CO₂ uptake enhancement induced by warmer springs. *Proceedings of the National Academy of Sciences of the United States of America*, *102*, 10823-10827
- Baldocchi, D., Falge, E., & Wilson, K. (2001). A spectral analysis of biosphere-atmosphere trace gas flux densities and meteorological variables across hour to multi-year time scales. *Agricultural and Forest Meteorology*, *107*, 1-27
- Beck, P.S.A., Atzberger, C., Hogda, K.A., Johansen, B., & Skidmore, A.K. (2006). Improved monitoring of vegetation dynamics at very high latitudes: A new method using MODIS NDVI. *remote sensing of environment*, *100*, 321-334
- Bolton, D.K., & Friedl, M.A. (2013). Forecasting crop yield using remotely sensed vegetation indices and crop phenology metrics. *Agricultural and Forest Meteorology*, *173*, 74-84
- Boyd, D.S., Almond, S., Dash, J., Curran, P.J., & Hill, R.A. (2011). Phenology of vegetation in Southern England from Envisat MERIS terrestrial chlorophyll index (MTCI) data. *International Journal of Remote Sensing*, *32*, 8421-8447
- Bradley, B.A., Jacob, R.W., Hermance, J.F., & Mustard, J.F. (2007). A curve fitting procedure to derive inter-annual phenologies from time series of noisy satellite NDVI data. *remote sensing of environment*, *106*, 137-145
- Campagnolo, M.L., Sun, Q.S., Liu, Y., Schaaf, C., Wang, Z.S., & Roman, M.O. (2016). Estimating the effective spatial resolution of the operational BRDF, albedo, and nadir reflectance products from MODIS and VIIRS. *remote sensing of environment*, *175*, 52-64
- Campbell, J.L., Rustad, L.E., Boyer, E.W., Christopher, S.F., Driscoll, C.T., Fernandez, I.J., Groffman, P.M., Houle, D., Kiekbusch, J., Magill, A.H., Mitchell, M.J., & Ollinger, S.V. (2009). Consequences of climate change for biogeochemical cycling in forests of northeastern North America. *Canadian Journal of Forest Research*, *39*, 264-284
- Chen, F., & Dudhia, J. (2001). Coupling an advanced land surface-hydrology model with the Penn State-NCAR MM5 modeling system. Part I: Model implementation and sensitivity. *Monthly Weather Review*, *129*, 569-585
- Chen, J., Jonsson, P., Tamura, M., Gu, Z.H., Matsushita, B., & Eklundh, L. (2004). A simple method for reconstructing a high-quality NDVI time-series data set based on the Savitzky-Golay filter. *remote sensing of environment*, *91*, 332-344
- Churkina, G., Schimel, D., Braswell, B.H., & Xiao, X.M. (2005). Spatial analysis of growing season length control over net ecosystem exchange. *Global Change Biology*, *11*, 1777-1787
- Cleland, E.E., Allen, J.M., Crimmins, T.M., Dunne, J.A., Pau, S., Travers, S.E., Zavaleta, E.S., & Wolkovich, E.M. (2012). Phenological tracking enables positive species responses to climate change. *Ecology*, *93*, 1765-1771
- Cleland, E.E., Chuine, I., Menzel, A., Mooney, H.A., & Schwartz, M.D. (2007). Shifting plant phenology in response to global change. *Trends in Ecology & Evolution*, *22*, 357-365

- Cooke, J.E.K., & Weih, M. (2005). Nitrogen storage and seasonal nitrogen cycling in *Populus*: bridging molecular physiology and ecophysiology. *New Phytologist*, *167*, 19-30
- de Beurs, K.M., & Henebry, G.M. (2004). Land surface phenology, climatic variation, and institutional change: Analyzing agricultural land cover change in Kazakhstan. *remote sensing of environment*, *89*, 497-509
- de Beurs, K.M., & Henebry, G.M. (2005a). Land surface phenology and temperature variation in the International Geosphere-Biosphere Program high-latitude transects. *Global Change Biology*, *11*, 779-790
- de Beurs, K.M., & Henebry, G.M. (2005b). A statistical framework for the analysis of long image time series. *International Journal of Remote Sensing*, *26*, 1551-1573
- de Beurs, K.M., & Henebry, G.M. (2008). Northern annular mode effects on the land surface phenologies of northern Eurasia. *Journal of Climate*, *21*, 4257-4279
- de Beurs, K.M., & Henebry, G.M. (2010). Spatio-temporal statistical methods for modeling land surface phenology. In I.L. Hudson, & M.R. Keatley (Eds.), *Phenological Research - Methods for Environmental and Climate Change Analysis* (pp. 177-208). New York: Spring
- de Jong, R., de Bruin, S., de Wit, A., Schaepman, M.E., & Dent, D.L. (2011). Analysis of monotonic greening and browning trends from global NDVI time-series. *remote sensing of environment*, *115*, 692-702
- Delbart, N., Kergoat, L., Le Toan, T., Lhermitte, J., & Picard, G. (2005). Determination of phenological dates in boreal regions using normalized difference water index. *remote sensing of environment*, *97*, 26-38
- Elmore, A.J., Guinn, S.M., Minsley, B.J., & Richardson, A.D. (2012). Landscape controls on the timing of spring, autumn, and growing season length in mid-Atlantic forests. *Global Change Biology*, *18*, 656-674
- EPA (2016). Climate Change Indicators in the United States, Fourth Edition In. <https://www.epa.gov/climate-indicators#explore>
- Ganguly, S., Friedl, M.A., Tan, B., Zhang, X.Y., & Verma, M. (2010). Land surface phenology from MODIS: Characterization of the Collection 5 global land cover dynamics product. *Remote Sensing of Environment*, *114*, 1805-1816
- Gao, F., Anderson, M.C., Zhang, X., Yang, Z., Alfieri, J.G., Kustas, W.P., Mueller, R., Johnson, D.M., & Prueger, J.H. (2017). Toward mapping crop progress at field scales through fusion of Landsat and MODIS imagery. *Remote Sens. Environ*, *188*, 9-25
- Gao, F., Masek, J., Schwaller, M., & Hall, F. (2006). On the blending of the Landsat and MODIS surface reflectance: Predicting daily Landsat surface reflectance. *Ieee Transactions on Geoscience and Remote Sensing*, *44*, 2207-2218
- Gerten, D., Schaphoff, S., Haberlandt, U., Lucht, W., & Sitch, S. (2004). Terrestrial vegetation and water balance - hydrological evaluation of a dynamic global vegetation model. *Journal of Hydrology*, *286*, 249-270
- Goetz, S.J., Bunn, A.G., Fiske, G.J., & Houghton, R.A. (2005). Satellite-observed photosynthetic trends across boreal North America associated with climate and fire disturbance. *Proceedings of the National Academy of Sciences of the United States of America*, *102*, 13521-13525

- Goward, S., Tucker, C., & Dye, D. (1985). North American vegetation patterns observed with the NOAA-7 Advanced Very High Resolution Radiometer. In *Vegetatio* (pp. 237-253)
- Goward, S.N., Markham, B., Dye, D.G., Dulaney, W., & Yang, A.J. (1991). Normalized difference vegetation index measurements from the Advanced Very High Resolution Radiometer. *remote sensing of environment*, *35*, 257-277
- Graham, E.A., Riordan, E.C., Yuen, E.M., Estrin, D., & Rundel, P.W. (2010). Public Internet-connected cameras used as a cross-continental ground-based plant phenology monitoring system. *Global Change Biology*, *16*, 3014-3023
- Gray, J.M., Frohling, S., Kort, E.A., Ray, D.K., Kucharik, C.J., Ramankutty, N., & Friedl, M.A. (2014). Direct human influence on atmospheric CO₂ seasonality from increased cropland productivity. *Nature*, *515*, 398+
- Hargrove, W.W., Spruce, J.P., Gasser, G.E., & Hoffman, F.M. (2009). Toward a National Early Warning System for Forest Disturbances Using Remotely Sensed Canopy Phenology. *Photogrammetric Engineering and Remote Sensing*, *75*, 1150-1156
- Heimann, M., Esser, G., Haxeltine, A., Kaduk, J., Kicklighter, D.W., Knorr, W., Kohlmaier, G.H., McGuire, A.D., Melillo, J., Moore, B., Otto, R.D., Prentice, I.C., Sauf, W., Schloss, A., Sitch, S., Wittenberg, U., & Wurth, G. (1998). Evaluation of terrestrial Carbon Cycle models through simulations of the seasonal cycle of atmospheric CO₂: First results of a model intercomparison study. *Global Biogeochemical Cycles*, *12*, 1-24
- Henebry, G.M., & de Beurs, K.M. (2013). Remote Sensing of Land Surface Phenology: A Prospectus. In M.D. Schwartz (Ed.), *Phenology: An Integrative Environmental Science* (pp. 385-411): Springer
- Herrmann, S.M., Anyamba, A., & Tucker, C.J. (2005). Recent trends in vegetation dynamics in the African Sahel and their relationship to climate. *Global Environmental Change-Human and Policy Dimensions*, *15*, 394-404
- Hickler, T., Eklundh, L., Seaquist, J.W., Smith, B., Ardo, J., Olsson, L., Sykes, M.T., & Sjoström, M. (2005). Precipitation controls Sahel greening trend. *Geophysical Research Letters*, *32*, -
- Hogg, E.H., Price, D.T., & Black, T.A. (2000). Postulated feedbacks of deciduous forest phenology on seasonal climate patterns in the western Canadian interior. *Journal of Climate*, *13*, 4229-4243
- Holben, B.N. (1986). Characteristics of maximum value composite images from temporal AVHRR data. In *International Journal of Remote Sensing* (pp. 1417-1434)
- Huete, A.R., Didan, K., Shimabukuro, Y.E., Ratana, P., Saleska, S.R., Hutya, L.R., Yang, W.Z., Nemani, R.R., & Myneni, R. (2006). Amazon rainforests green-up with sunlight in dry season. *Geophysical Research Letters*, *33*
- Hufkens, K., Friedl, M., Sonnentag, O., Braswell, B.H., Milliman, T., & Richardson, A.D. (2012). Linking near-surface and satellite remote sensing measurements of deciduous broadleaf forest phenology. *remote sensing of environment*, *117*, 307-321
- IPCC (2007). Contribution of working group II to the fourth assessment report of the Intergovernmental Panel on Climate Change. In M. L. Parry et al. (Ed.), *Climate*

- Change 2007: Impacts, Adaptation, and Vulnerability* (p. 976). Cambridge: Cambridge Univ. Press
- IPCC (2014). Climate Change 2014: Synthesis Report. Contribution of Working Groups I, II and III to the Fifth Assessment Report of the Intergovernmental Panel on Climate Change In R.K. Pachauri, & L.A. Meyer (Eds.) (p. 151). Geneva, Switzerland
- Ivits, E., Cherlet, M., Toth, G., Sommer, S., Mehl, W., Vogt, J., & Micale, F. (2012). Combining satellite derived phenology with climate data for climate change impact assessment. *Global and Planetary Change*, 88-89, 85-97
- Jakubauskas, M.E., Legates, D.R., & Kastens, J.H. (2001). Harmonic analysis of time-series AVHRR NDVI data. *Photogrammetric Engineering and Remote Sensing*, 67, 461-470
- Jiang, Z.Y., Huete, A.R., Didan, K., & Miura, T. (2008). Development of a two-band enhanced vegetation index without a blue band. *remote sensing of environment*, 112, 3833-3845
- Jonsson, P., & Eklundh, L. (2002). Seasonality extraction by function fitting to time-series of satellite sensor data. *Ieee Transactions on Geoscience and Remote Sensing*, 40, 1824-1832
- Ju, J.C., & Roy, D.P. (2008). The availability of cloud-free Landsat ETM plus data over the conterminous United States and globally. *remote sensing of environment*, 112, 1196-1211
- Justice, C., Townshend, J., Holben, B., & Tucker, C. (1985). Analysis of the phenology of global vegetation using meteorological satellite data. *International Journal of Remote Sensing*, 6, 1271-1318
- Keenan, T.F., Darby, B., Felts, E., Sonnentag, O., Friedl, M.A., Hufkens, K., O'Keefe, J., Klosterman, S., Munger, J.W., Toomey, M., & Richardson, A.D. (2014a). Tracking forest phenology and seasonal physiology using digital repeat photography: a critical assessment. *Ecological Applications*, 24, 1478-1489
- Keenan, T.F., Gray, J., Friedl, M.A., Toomey, M., Bohrer, G., Hollinger, D.Y., Munger, J.W., O'Keefe, J., Schmid, H.P., SueWing, I., Yang, B., & Richardson, A.D. (2014b). Net carbon uptake has increased through warming-induced changes in temperate forest phenology. *Nature Climate Change*, 4, 598-604
- Klosterman, S.T., Hufkens, K., Gray, J.M., Melaas, E., Sonnentag, O., Lavine, I., Mitchell, L., Norman, R., Friedl, M.A., & Richardson, A.D. (2014). Evaluating remote sensing of deciduous forest phenology at multiple spatial scales using PhenoCam imagery. *Biogeosciences*, 11, 4305-4320
- Korner, C., & Basler, D. (2010). Phenology Under Global Warming. *Science*, 327, 1461-1462
- Krehbiel, C.P., Jackson, T., & Henebry, G.M. (2016). Web-Enabled Landsat Data Time Series for Monitoring Urban Heat Island Impacts on Land Surface Phenology. *Ieee Journal of Selected Topics in Applied Earth Observations and Remote Sensing*, 9, 2043-2050
- Melaas, E.K., Friedl, M.A., & Zhu, Z. (2013). Detecting interannual variation in deciduous broadleaf forest phenology using Landsat TM/ETM plus data. *remote sensing of environment*, 132, 176-185

- Melaas, E.K., Wang, J.A., Miller, D.L., & Friedl, M.A. (2016). Interactions between urban vegetation and surface urban heat islands: a case study in the Boston metropolitan region. *Environmental Research Letters*, 11
- Moody, A., & Johnson, D.M. (2001). Land-surface phenologies from AVHRR using the discrete fourier transform. *remote sensing of environment*, 75, 305-323
- Moore, K.E., Fitzjarrald, D.R., Sakai, R.K., Goulden, M.L., Munger, J.W., & Wofsy, S.C. (1996). Seasonal variation in radiative and turbulent exchange at a deciduous forest in central Massachusetts. *Journal of Applied Meteorology*, 35, 122-134
- Morisette, J.T., Richardson, A.D., Knapp, A.K., Fisher, J.I., Graham, E.A., Abatzoglou, J., Wilson, B.E., Breshears, D.D., Henebry, G.M., Hanes, J.M., & Liang, L. (2009). Tracking the rhythm of the seasons in the face of global change: phenological research in the 21st century. *Frontiers in Ecology and the Environment*, 7, 253-260
- Moulin, S., Kergoat, L., Viovy, N., & Dedieu, G. (1997). Global-scale assessment of vegetation phenology using NOAA/AVHRR satellite measurements. *Journal of Climate*, 10, 1154-1170
- Myneni, R.B., Keeling, C.D., Tucker, C.J., Asrar, G., & Nemani, R.R. (1997). Increased plant growth in the northern high latitudes from 1981 to 1991. *Nature*, 386, 698-702
- Ollinger, S.V., Richardson, A.D., Martin, M.E., Hollinger, D.Y., Frohling, S.E., Reich, P.B., Plourde, L.C., Katul, G.G., Munger, J.W., Oren, R., Smith, M.L., U, K.T.P., Bolstad, P.V., Cook, B.D., Day, M.C., Martin, T.A., Monson, R.K., & Schmid, H.P. (2008). Canopy nitrogen, carbon assimilation, and albedo in temperate and boreal forests: Functional relations and potential climate feedbacks. *Proceedings of the National Academy of Sciences of the United States of America*, 105, 19336-19341
- Olsson, L., Eklundh, L., & Ardo, J. (2005). A recent greening of the Sahel - Trends, patterns and potential causes. *Journal of Arid Environments*, 63, 556-566
- Parmesan, C., & Yohe, G. (2003). A globally coherent fingerprint of climate change impacts across natural systems. *Nature*, 421, 37-42
- Puma, M.J., Koster, R.D., & Cook, B.I. (2013). Phenological versus meteorological controls on land-atmosphere water and carbon fluxes. *Journal of Geophysical Research-Biogeosciences*, 118, 14-29
- Reed, B.C., Brown, J.F., Vanderzee, D., Loveland, T.R., Merchant, J.W., & Ohlen, D.O. (1994a). Measuring Phenological Variability from Satellite Imagery. *Journal of Vegetation Science*, 5, 703-714
- Reed, B.C., Brown, J.F., VanderZee, D., Loveland, T.R., Merchant, J.W., & Ohlen, D.O. (1994b). Measuring phenological variability from satellite imagery. *Journal of Vegetation Science*, 5, 703-714
- Richardson, A.D., Braswell, B.H., Hollinger, D.Y., Jenkins, J.P., & Ollinger, S.V. (2009a). Near-surface remote sensing of spatial and temporal variation in canopy phenology. *Ecological Applications*, 19, 1417-1428
- Richardson, A.D., Hollinger, D.Y., Dail, D.B., Lee, J.T., Munger, J.W., & O'Keefe, J. (2009b). Influence of spring phenology on seasonal and annual carbon balance in two contrasting New England forests. *Tree Physiology*, 29, 321-331
- Richardson, A.D., Jenkins, J.P., Braswell, B.H., Hollinger, D.Y., Ollinger, S.V., & Smith, M.L. (2007). Use of digital webcam images to track spring green-up in a deciduous broadleaf forest. *Oecologia*, 152, 323-334

- Richardson, A.D., Keenan, T.F., Migliavacca, M., Ryu, Y., Sonnentag, O., & Toomey, M. (2013). Climate change, phenology, and phenological control of vegetation feedbacks to the climate system. *Agricultural and Forest Meteorology*, *169*, 156-173
- Rodriguez-Galiano, V.F., Dash, J., & Atkinson, P.M. (2015). Characterising the Land Surface Phenology of Europe Using Decadal MERIS Data. *Remote Sensing*, *7*, 9390-9409
- Schaaf, C.B., Gao, F., Strahler, A.H., Lucht, W., Li, X.W., Tsang, T., Strugnell, N.C., Zhang, X.Y., Jin, Y.F., Muller, J.P., Lewis, P., Barnsley, M., Hobson, P., Disney, M., Roberts, G., Dunderdale, M., Doll, C., d'Entremont, R.P., Hu, B.X., Liang, S.L., Privette, J.L., & Roy, D. (2002). First operational BRDF, albedo nadir reflectance products from MODIS. *remote sensing of environment*, *83*, 135-148
- Schaaf, C.B., Liu, J., Gao, F., & Strahler, A.H. (2011). MODIS albedo and reflectance an isotropy products from Aqua and Terra. In B. Ramachandran, C. Justice, & M. Abrams (Eds.), *Land Remote Sensing and Global Environmental Change: NASA's Earth Observing System and the Science of ASTER and MODIS* (pp. 549-562): Springer-Cerlag
- Seaquist, J.W., Olsson, L., Ardo, J., & Eklundh, L. (2006). Broad-scale increase in NPP quantified for the African Sahel, 1982-1999. *International Journal of Remote Sensing*, *27*, 5115-5122
- Sonnentag, O., Hufkens, K., Teshera-Sterne, C., Young, A.M., Friedl, M., Braswell, B.H., Milliman, T., O'Keefe, J., & Richardson, A.D. (2012). Digital repeat photography for phenological research in forest ecosystems. *Agricultural and Forest Meteorology*, *152*, 159-177
- Tan, B., Morisette, J.T., Wolfe, R.E., Gao, F., Ederer, G.A., Nightingale, J., & Pedelty, J.A. (2011). An Enhanced TIMESAT Algorithm for Estimating Vegetation Phenology Metrics From MODIS Data. *Ieee Journal of Selected Topics in Applied Earth Observations and Remote Sensing*, *4*, 361-371
- Thompson, D., & Wehmanen, O. (1979). Using Landsat Digital Data to Detect Moisture Stress. *Photogrammetric Engineering and Remote-sensing* *45*, 201-207
- USGCRP (2010). Ecosystem Responses to Climate Change: Selecting Indicators and Integrating Observational Networks. In *NCA Report Series, 5a*. Washington, DC, <http://data.globalchange.gov/assets/68/23/2165abcb9561c165fb65ec2dcf3a/ecological-indicators-workshop-report.pdf>
- USGCRP (2015). National Climate Assessment & Development Advisory Committee (2011–2014) Meetings, decisions, and adopted documents. In <http://www.globalchange.gov/what-we-do/assessment/ncadac>
- van Leeuwen, W.J.D., Huete, A.R., & Laing, T.W. (1999). MODIS vegetation index compositing approach: A prototype with AVHRR data. *remote sensing of environment*, *69*, 264-280
- Verstraete, M.M., Gobron, N., Aussedat, O., Robustelli, M., Pinty, B., Widlowski, J.L., & Taberner, M. (2008). An automatic procedure to identify key vegetation phenology events using the JRC-FAPAR products. *Advances in Space Research*, *41*, 1773-1783

- Viovy, N., Arino, O., & Belward, A.S. (1992). The Best Index Slope Extraction (Bise) - a Method for Reducing Noise in Ndvi Time-Series. *International Journal of Remote Sensing*, 13, 1585-1590
- Vivoni, E.R. (2012). Diagnosing Seasonal Vegetation Impacts on Evapotranspiration and Its Partitioning at the Catchment Scale during SMEX04-NAME. *Journal of Hydrometeorology*, 13, 1631-1638
- Walther, G.R. (2010). Community and ecosystem responses to recent climate change. *Philosophical Transactions of the Royal Society B-Biological Sciences*, 365, 2019-2024
- White, M.A., de Beurs, K.M., Didan, K., Inouye, D.W., Richardson, A.D., Jensen, O.P., O'Keefe, J., Zhang, G., Nemani, R.R., van Leeuwen, W.J.D., Brown, J.F., de Wit, A., Schaepman, M., Lin, X.M., Dettinger, M., Bailey, A.S., Kimball, J., Schwartz, M.D., Baldocchi, D.D., Lee, J.T., & Lauenroth, W.K. (2009). Intercomparison, interpretation, and assessment of spring phenology in North America estimated from remote sensing for 1982-2006. *Global Change Biology*, 15, 2335-2359
- White, M.A., Thornton, P.E., & Running, S.W. (1997). A continental phenology model for monitoring vegetation responses to interannual climatic variability. *Global Biogeochemical Cycles*, 11, 217-234
- Williamson, S.N., Barrio, I.C., Hik, D.S., & Gamon, J.A. (2016). Phenology and species determine growing-season albedo increase at the altitudinal limit of shrub growth in the sub-Arctic. *Global Change Biology*
- Willmott, C.J. (1981). On the validation of models. *Physical Geography*, 2, 184-194
- Wolkovich, E.M., Cook, B.I., Allen, J.M., Crimmins, T.M., Betancourt, J.L., Travers, S.E., Pau, S., Regetz, J., Davies, T.J., Kraft, N.J.B., Ault, T.R., Bolmgren, K., Mazer, S.J., McCabe, G.J., McGill, B.J., Parmesan, C., Salamin, N., Schwartz, M.D., & Cleland, E.E. (2012). Warming experiments underpredict plant phenological responses to climate change. *Nature*, 485, 494-497
- Zeng, H.Q., Jia, G.S., & Forbes, B.C. (2013). Shifts in Arctic phenology in response to climate and anthropogenic factors as detected from multiple satellite time series. *Environmental Research Letters*, 8
- Zhang, X., Friedl, M., & Schaaf, C. (2009). Sensitivity of vegetation phenology detection to the temporal resolution of satellite data. *International Journal of Remote Sensing*, 30, 2061-2074
- Zhang, X.Y. (2015). Reconstruction of a complete global time series of daily vegetation index trajectory from long-term AVHRR data. *remote sensing of environment*, 156, 457-472
- Zhang, X.Y., Friedl, M.A., & Schaaf, C.B. (2006). Global vegetation phenology from Moderate Resolution Imaging Spectroradiometer (MODIS): Evaluation of global patterns and comparison with in situ measurements. *Journal of Geophysical Research-Biogeosciences*, 111
- Zhang, X.Y., Friedl, M.A., Schaaf, C.B., Strahler, A.H., Hodges, J.C.F., Gao, F., Reed, B.C., & Huete, A. (2003). Monitoring vegetation phenology using MODIS. *Remote Sensing of Environment*, 84, 471-475
- Zhang, X.Y., Tan, B., & Yu, Y.Y. (2014). Interannual variations and trends in global land surface phenology derived from enhanced vegetation index during 1982-2010. *International Journal of Biometeorology*, 58, 547-564

- Zhang, X.Y., Tarpley, D., & Sullivan, J.T. (2007). Diverse responses of vegetation phenology to a warming climate. *Geophysical Research Letters*, *34*
- Zhou, L.M., Tian, Y.H., Myneni, R.B., Ciais, P., Saatchi, S., Liu, Y.Y., Piao, S.L., Chen, H.S., Vermote, E.F., Song, C.H., & Hwang, T.H. (2014). Widespread decline of Congo rainforest greenness in the past decade. *Nature*, *509*, 86-+
- Zhou, L.M., Tucker, C.J., Kaufmann, R.K., Slayback, D., Shabanov, N.V., & Myneni, R.B. (2001). Variations in northern vegetation activity inferred from satellite data of vegetation index during 1981 to 1999. *Journal of Geophysical Research-Atmospheres*, *106*, 20069-20083